LAPPEENRANTA UNIVERSITY OF TECHNOLOGY

Faculty of Technology

Master's Degree Programme in Technomathematics and Technical Physics

Maksim Zinchenko

TRANSIENT CURRENT TECHNIQUE SIMULATION OF SEMICONDUCTOR DETECTORS

Supervising Professor /

First Examiner: Ph.D. / Professor Tuure Tuuva

Second Examiner: Ph.D. / Associate Professor Erik Vartiainen

ABSTRACT

Lappeenranta University of Technology
Faculty of Technology
Technomathematics and Technical Physics

Maksim Zinchenko

Transient Current Technique Simulation of Semiconductor Detectors

Master's thesis

2014

50 pages, 28 figures and 3 appendices

Examiners: Ph.D. Tuure Tuuva
Ph.D. Erik Vartiainen

Keywords: silicon detectors, transient current technique (TCT), TCAD, ATLAS, ATHENA, SILAVACO, MixedMode.

Nowadays advanced simulation technologies of semiconductor devices occupies an important place in microelectronics production process. Simulation helps to understand devices internal processes physics, detect new effects and find directions for optimization. Computer calculation reduces manufacturing costs and time.

Modern simulation suits such as Silcaco TCAD allow simulating not only individual semiconductor structures, but also these structures in the circuit. For that purpose TCAD include MixedMode tool. That tool can simulate circuits using compact circuit models including semiconductor structures with their physical models.

In this work, MixedMode is used for simulating transient current technique setup, which include detector and supporting electrical circuit. This technique was developed by RD39 collaboration project for investigation radiation detectors radiation hard properties.

ACKNOWLEDGEMENTS

I would like to thank my supervising professor in Lappeenranta University of Technology Tuure Tuuva for great possibility to choose and write that work. Moreover, I am very grateful to Maria Golovleva for teaching working with TCAD simulation framework and exploration TCT theory.

I would like to thank Erkki Lahderanta and Erik Vartiainen for their huge assistance during all double degree Master's Program in Technical Physics and for their great lectures in Lappeenranta University of Technology.

I would also like to thank professors and lecturers in my home university – Moscow Power Engineering Institute for good fundamental knowledge that they give to me.

For me it was good experience to get knowledge about Silvaco simulation software. I am proud that my work connected with detectors used in the Large Hadron Collider. I am sure that I have done important work and it will be helpful for future researchers.

CONTENTS

LIST OF SYMBOLS AND ABBREVIATIONS

Symbols

N_A	density of acceptor impurity atoms
N_D	density of donor impurity atoms
$-x_p$	limit of depletion region on p-side
x_n	limit of depletion region on n-side
E_F	Fermi energy level
V_{bi}	built in potential
E_v	energy level of valence band
E_c	energy level of conduction band
ρ	electric charge density
ε_s	permittivity of semiconductor
q	elementary charge
$E_{\max}$	maximum electric field
W	width of depletion region
D	thickness of detector
V_{fd}	voltage of full depletion
C	capacitance
Q_c	charge per unit area
A	active area of detector
J_s	saturation current
D_p	diffusion constant of holes
D_n	diffusion constant of electrons
p_{n0}	density of holes on the n-side in equilibrium
n_{p0}	density of electrons on the p-side in equilibrium
L_p	diffusion length of holes
L_n	diffusion length of electrons
J_{gen}	generation current
n_i	intrinsic carrier concentration
τ_{gen}	generation lifetime
N_C	density of states in the conduction band
N_V	density of states in the valence band
E_g	band gap energy
k_B	Bolzmann’s constant
n	density of electrons
p	density of holes
μ_n	mobility of electrons
μ_p	mobility of holes

J_n	electron current density
J_p	hole current density
τ_{eff}	effective trapping time constant
v_{dr}	charge carrier velocity
E_v	electric field caused by unit potential
t_{dr}	drifting time
n_0	injected electron density
$i(t)$	transient current
$E(x)$	electric field
$I(t)$	detector current
Q	collected charge
CCE	charge collection efficiency
CCE_g	geometrical factor of CCE
CCE_t	trapping induced factor of CCE
φ	electrostatic potential
G_n	generation rates for electrons
R_n	recombination rates for electrons
G_p	generation rates for holes
R_p	recombination rates for holes

Abbreviations

ALICE	A Large Ion Collider Experiment
ATLAS	A Toroidal LHC Apparatus
CCE	charge collection efficiency
CERN	European Organization for Nuclear Research
CID	current injected detector
CMS	Compact Muon Solenoid
HEP	high energy physics
LHC	Large Hadron Collider
RD39	CERN Collaboration: Cryogenic Tracking Detectors
RD48	CERN Collaboration: Research and development On Silicon for future Experiments (ROSE)
RD50	CERN Collaboration: Radiation hard semiconductor devices for very high luminosity colliders
SCR	space charge region
TCT	Transient Current Technique

1. INTRODUCTION

At the 10 September of 2008 after twenty years of planning and ten years of construction, the first beam starts circulate in the world's largest and most powerful particle accelerator - Large Hadron Collider (LHC) build by the European Organization for Nuclear Research CERN. It was built to check the predictions of various theories of particle physics and find the theorized Higgs particle. LHC allows to reach larger energy of circulated particles and has new devices and methods to explore particle properties. It has considerable importance for international scientific community in the field of experimental high-energy physics (HEP) [1]. The Large Hadron Collider is illustrated in Figure 1.

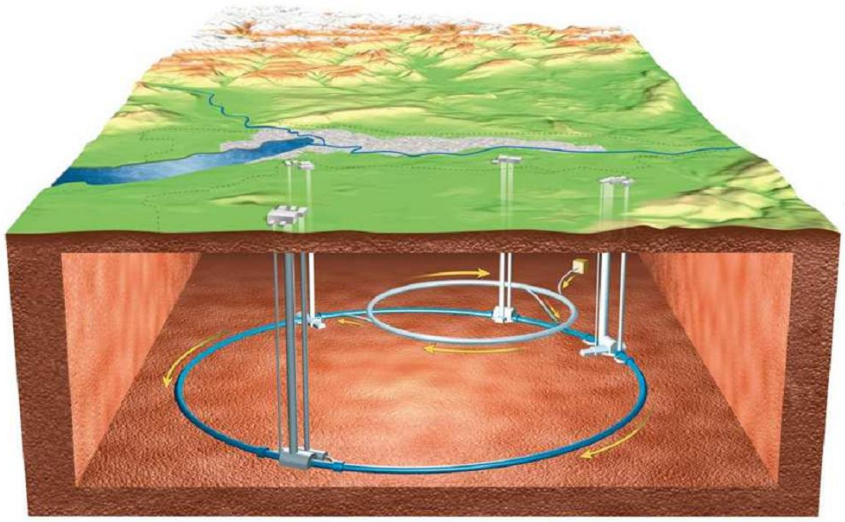

Figure 1: The Large Hadron Collider [1].

Nowadays the Standard Model is main theory of all particle physics. The Higgs boson is the key building block in this model. This is massive scalar elementary particle theorized by Peter Higgs [2]. According to his theory, it was predicted that both carrier particles and matter particles interact.

The discovery of the Higgs boson was announced on 4 July 2012 by ATLAS and CMS team at the Large Hadron Collider and was called “monumental” [3], on 14 March 2013 this discovery was confirmed. Discovered mass of the Higgs boson is about

125.5 GeV/c^2 - rather heavy particle. Predicted in the standard model mean lifetime is $1.56 \times 10^{-22}\ s$.

The Larger Hadron Collider consist of an accelerator ring that includes 9300 magnets. This ring is located 100 meters underground in a 27 kilometers long tunnel. Particles could be accelerated around the circle in both directions in separate beam pipes. There are two major types of accelerated particles: protons and lead ions. Magnets used in the Large Hadron Collider are based on superconducting principle, because high magnetic field is needed to focus the particle beam. Hence, it is required to achieve very low temperature to operate accelerator magnets. Particle beams could achieve the speed close to light velocity. The energy of single particle reaches up to 7 TeV [4].

There are four main experimental parts of the LHC where occurs collisions between particles: CMS, ATLAS, ALICE and LHCb. The Compact Muon Solenoid (CMS) detector is a general-purpose detector that is shown in Figure 2. The CMS is designed for detect any appearing particles with high energies. Experiments with particle decays in that energy range could help in verification physical theories. This detector also could search the Higgs boson, and gives large data for researcher of dark matter, antimatter and string theory [5].

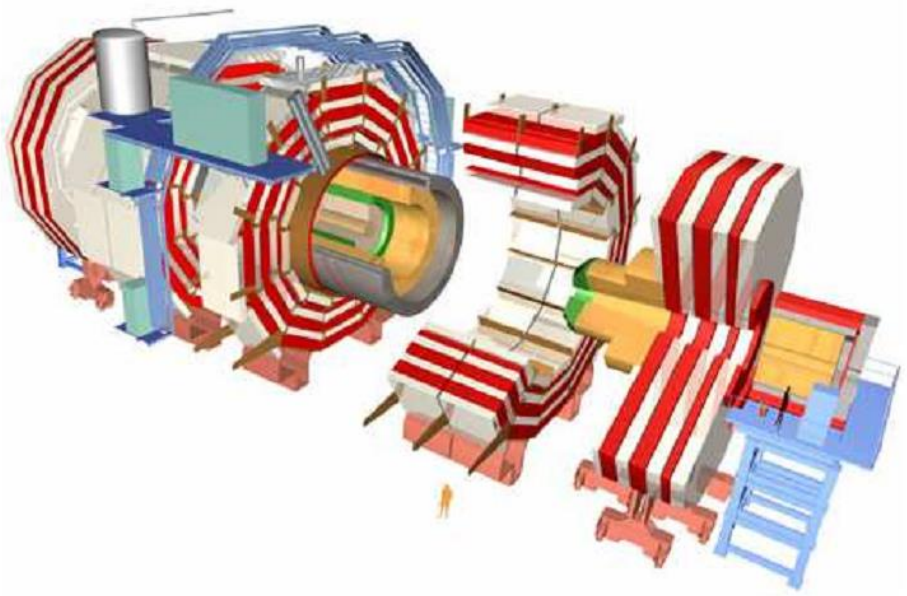

Figure 2: Schematic view of the whole Compact Muon Solenoid Detector [6].

The CMS consists of many parts that are needed to determine different particles. There are the tracker for identifying particle tracks, two type of calorimeters and muon system, which could detects their tracks [6]. The all-silicon tracker system in Compact Muon Solenoid detector include detectors based on different principles [7]. Pixel detectors provide highest spatial resolution. That is why they are installed closest to the particle interaction point. Next layer is located behind pixel detectors and consists of silicon strip detectors. Very extensive particle radiation expose silicon tracker system. The installation of that system is shown in Figure 3.

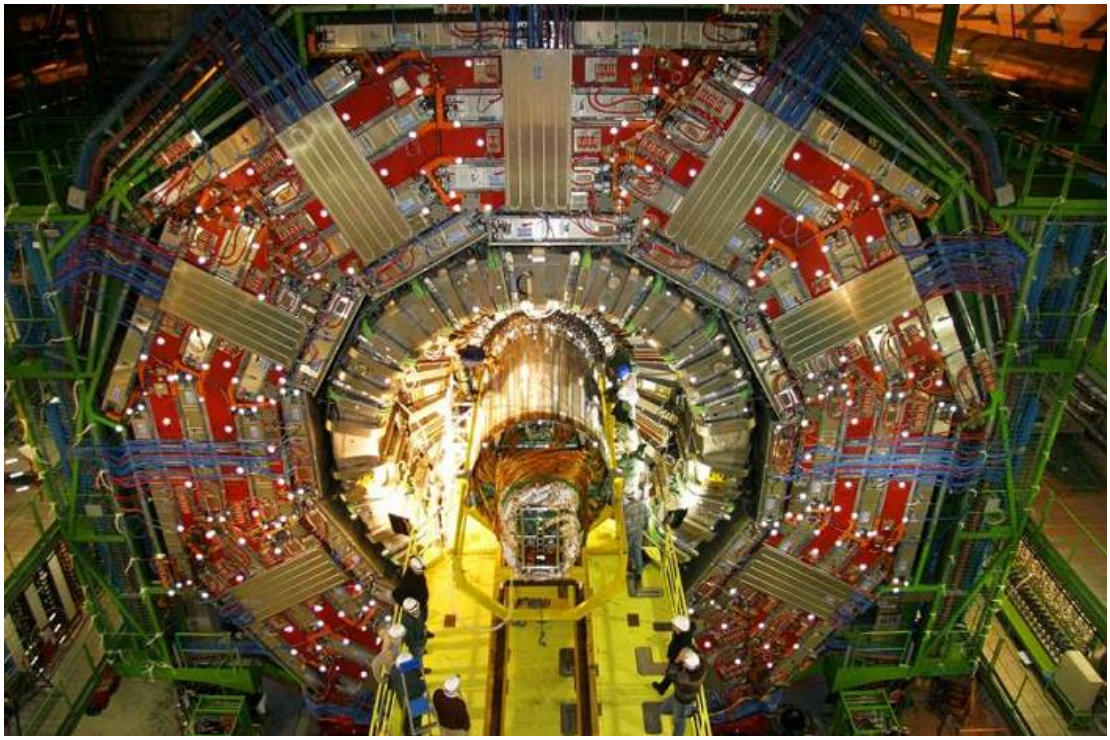

Figure 3: Installation of the CMS tracker [7].

The radiation cause the deterioration of performance in silicon detectors. The ability to withstand that process is called radiation hardness. It is calculated that pixel detectors installed in CMS achieve the limits of their functionality within the next five years and strip detectors will be functional for approximately ten years. Detectors functionality limitations are caused by extensive particle radiation described earlier

One of the main method for examining detectors is the Transient Current Technique (TCT) that has been developed by researchers of the Ioffe Institute and the Brookhaven National Laboratory [8]. The method has several advantages: it is more

efficient than traditional C–V measurements for highly irradiated structures and this method is nondestructive. Different parameters of the detector could be extracted using this technique, such as the voltage of full depletion, charge collection efficiency and effective trapping time.

This thesis project focuses on simulation TCT measurements setup in TCAD framework. Transient current technique simulation of basic detector and conventional p-type strip detector are carried out.

The theoretical background for p-n junction and silicon particle detector are presented in Chapter 2. Chapter 3 concentrates on the method of TCT describing the principle of the technique and measurement setup. In the Chapter 4 is devoted to TCAD framework and mathematical models used in this software. The results of TCT simulation in MixedMode tool are presented in Chapter 5. Chapter 6 summarizes the contents.

2. SILCON DETECTORS

The Large Hadron Collider has silicon particles detectors, which are based on principle of reverse biased p-n diodes. When the bias voltage is applied, the electric field extends over the whole detector thickness. Ionizing particles, which go through the detector, generate electron-hole pairs along their path in the bulk of the silicon. The reverse electric field moves these free charge carriers to opposite sides of the detector and they are collected there. Silicon detectors are good choice for monitoring in a high interaction rate environment because they have low electron-hole pair creation energy and high time of charge collections. The following chapters are based on book S. M. Sze. "Physics of semiconductor devices" [9].

2.1 p-n Junction

In silicon, amount of no equilibrium electrons and holes can be controlled by doping the structure by donors or acceptors. When impurity atoms replace some of Si atoms in the lattice, it creates energy levels near valence or conduction band. These levels are called shallow levels. Donors are impurity atoms, which have one electron more than atoms of host material. They donate this electron to the conduction band and, in this case, donor atom becomes positive ion. Acceptors are impurity atoms, which have one electron less than atoms of host material. They can accept an electron from the valence band and create there a hole. After that acceptor atom becomes negatively charged.

When the impurity concentration in a semiconductor changes abruptly from acceptor impurities N_A to donor impurities N_D as shown in Figure 4a, it creates an abrupt junction combined of two independent parts: one part is p-type and the other is n-type. In the case of higher impurity density on one side of the junction, than on the other side (for example $N_A \gg N_D$), one obtains a one-side abrupt p^+-n (or n^+-p) junction. After creation common interface between p-type and n-type regions, free electrons from n-side and holes from p-side diffuse to the other side of the junction, where they recombine, until structure get thermal equilibrium. Electrons go to p-side, leave their positions in n-type regions and create donor ions behind until x_n (Figure 4b). Holes migration leaves p region with a net of negative charge acceptor ions until x_p (Figure 4b). The region between $-x_p$ and x_n is called the depletion region or space charge region (SCR). It is empty of free charge

carriers and contain negatively and positively ions. After achieving new equilibrium state current flow stops.

Concentration of impurities influences on Fermi energy level E_F, in p-type semiconductor it moves close to the valence band E_v and to the conduction band E_c in n-type semiconductor. The condition of zero current flow requires that the Fermi level must be constant over the whole structure. That condition leads to a build-in potential V_{bi}, which could be described as the corresponding potential to the electric field that is created in space charge region between ionized ions opposite charge. The Figure 4d shows distribution of potential over the whole structure.

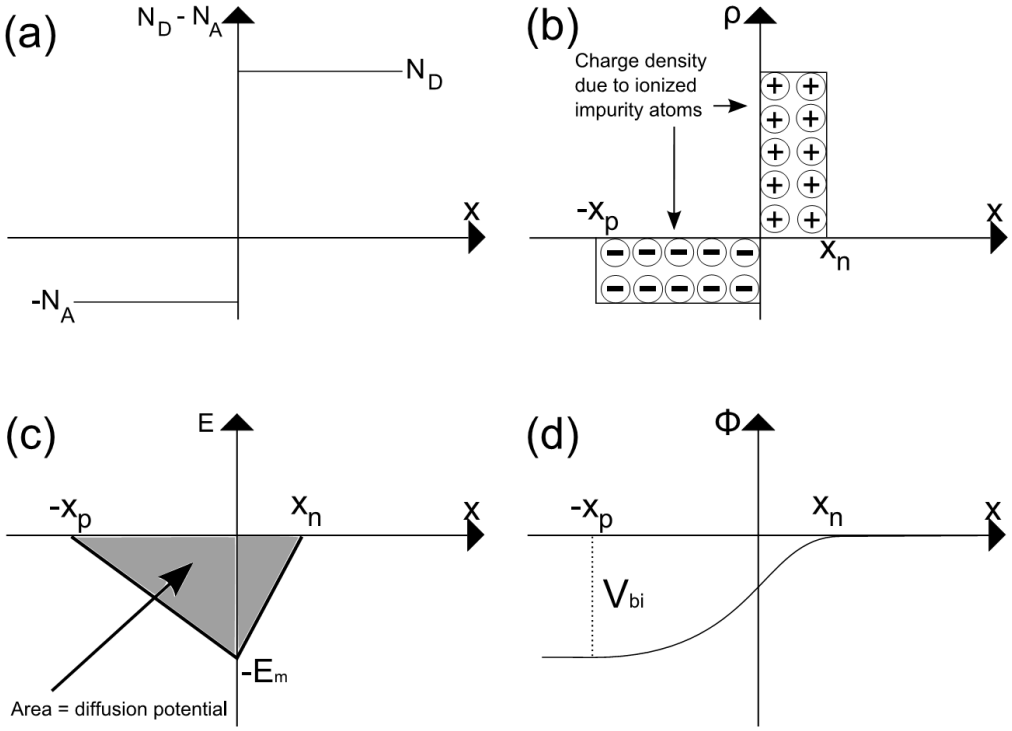

Figure 4: Abrupt p-n junction: a) density of impurity atoms; b) charge density due to ionized impurity atoms; c) electric field over the structure; d) distribution of potential over the junction.

The electrical properties of the p-n junction could be described mathematically from the Poisson equation:

$$\frac{dE}{dx} = \frac{\rho}{\varepsilon_s} \tag{1}$$

The electric charge density ρ could be found from the corresponding impurity atom concentration (in the case of ionization of all impurity atoms): for acceptor doping $-qN_A$ and qN_D for donors. Equation 1 could be rewritten in the following way:

$$-\frac{d^2V}{dx^2} = \frac{qN_D}{\varepsilon_s} \text{ for } 0 < x \leq x_n \tag{2}$$

$$\frac{d^2V}{dx^2} = \frac{qN_A}{\varepsilon_s} \text{ for } -x_p < x \leq 0 \tag{3}$$

Figure 4c shows that the maximum of the electric field is located at $x = 0$ and it is equal zero at $-x_p$ and x_n. The distribution of the electric field could be obtained by integrating the above equations:

$$E(x) = -\frac{qN_D}{\varepsilon_s}(x_n - x) \text{ for } 0 < x \leq x_n \tag{4}$$

$$E(x) = -\frac{qN_A(x + x_p)}{\varepsilon_s} \text{ for } -x_p < x \leq 0 \tag{5}$$

The maximum electric field that exists at $x = 0$ is given by

$$|E_{\max} \quad (x = 0)| = \frac{qN_A x_p}{\varepsilon_s} = \frac{qN_D x_n}{\varepsilon_s} \tag{6}$$

The build-in potential could be found by integrating equations 2 and 3 twice

$$V_{bi} = \frac{1}{2}\frac{qN_A}{\varepsilon_s}x_p^2 - \frac{1}{2}\frac{qN_D}{\varepsilon_s}x_n^2 = -\frac{1}{2}E_{max}(x_p + x_n) = -\frac{1}{2}E_{max}W \tag{7}$$

Where W is the depletion width that is distance from $-x_p$ to x_n. Value of $-x_p$ and x_n could be obtained by solving equation 6, that could give

$$x_c + x_p = E_{max}\frac{\varepsilon_s}{q}\left(\frac{1}{N_A} + \frac{1}{N_D}\right) \tag{8}$$

After obtaining E_{max} from equation 6, previous equation could be rewritten in following way:

$$W = \sqrt{\frac{2\varepsilon_s V_{bi}}{q}}\left(\frac{N_A + N_D}{N_A N_D}\right) \tag{9}$$

In the case of one-side n^+-p junction where $N_D \gg N_A$, it means that the majority of the potential variation and depletion region will be inside the lightly doped side [9].

Equation 9 reduces to

$$W = \sqrt{\frac{2\varepsilon_s V_{bi}}{qN_A}} \tag{10}$$

On the other hand, if concentration of acceptor impurities more than donor ones $N_A \gg N_D$ the calculation will be the same and depletion width will extends to the side with donor doping. In many cases for detectors, it is important when the depletion width increase to the whole detector thickness D. That condition is achieved by applying to the detector reverse bias; this voltage is named full depletion voltage V_{fd}. Hence, equation 10 could be rewritten for one-side p-type structure, where $W = D$.

$$V_{bi} - V_{fd} = \frac{qN_A D^2}{2\varepsilon_s} \tag{11}$$

Equation 11 shows that there are two opportunities to get low full depletion voltage: decrease of detector thickness or impurity concentration. Another way is connected with changing the material of the structure, it will change V_{bi} and ε_s.

The depletion layer capacitance per unit area is defined as

$$C \equiv \frac{dQ_c}{dV} = \frac{\varepsilon_s}{W} \tag{12}$$

where dQ_c is the incremental depletion charge on each side of the junction (total charge is zero) upon an incremental charge of the applied voltage dV. For one-side abrupt junctions, the capacitance per unit area is given by [9]

$$C = \frac{\varepsilon_s}{W} = \sqrt{\frac{q\varepsilon_s N_A}{2(V_{bi} - V)}}, \qquad W \le D, V \le V_{fd} \tag{13}$$

In the case of fully depleted detector, the depletion layer capacitance per unit area is determined only by geometry of the structure:

$$C = \frac{\varepsilon_s A}{D} \tag{14}$$

where A is an active area of the diode. The C-V characteristic can give full depletion voltage V_{fd}.

Saturated diffusion current is defined by the ideal diode current law:

$$J_s = \frac{qD_p p_{n0}}{L_p} + \frac{qD_n n_{p0}}{L_n} \tag{15}$$

where D_n and D_p are diffusion constants for electrons and holes, L_n and L_p are diffusion length of free charge carriers, n_{p0} and p_{n0} are equilibrium densities on n-side and p-side.

If the detector is biasing by reverse voltage, the generation current J_{gen}, which is occurred in depletion region, could be calculated by:

$$J_{gen} = \frac{qn_i W}{\tau_{gen}} \tag{16}$$

where lifetime is determined by τ_{gen} and n_i is the carrier concentration in the intrinsic semiconductor, that could be fiend from:

$$n_i^2 = np = N_C N_V e^{\frac{-E_g}{k_B T}} \tag{17}$$

In the equation 17, E_g is the band gap of the semiconductor, Bolzmann constant is determined by k_B, T – the temperature and N_C (N_V) are effective densities of states for conduction (valence) band.

When detector (diode) is applied low reverse bias voltage, there are several components in total reverse leakage current. First, the generation current takes place in depletion region of the structure. Second, the diffusion current occurs in the areas of the device where no space charge region is. Third, total leakage current is affected by parasitic currents; one of them is surface generation current.

On the other hand, when detector is fully depleted, total leakage current is defined only by the generation current J_{gen} (equation 16). It should be considered that, although lifetime of generated charge carriers τ_{gen} has weak dependence from temperature, but equation 17 shows that n_i is strongly temperature dependent. Hence, the generation current when detectors are fully depleted, also has strong dependence from temperature.

2.2 Particle Detectors

A diode in the detecting regime, than a reverse bias is applied to a semiconductor structure. In the Large Hadron Collider clashes are appeared in 25 nanosecond periods of time, and the detector signals should be processed in these short intervals of time. Detecting device is based on drift current is fast enough to split signals in short intervals. Hence, there is only one way to do this – measure drift current.

Usually detectors are semiconductor structures based on n-type bulk silicon substrate, which is highly doped from both sides by implantations. The front side of the detector is highly doped with acceptor type impurities that forms p^+-type implantation and strongly asymmetrical junction with n-type bulk substrate. This junction can be explained using the theory of the one-side junction, which was presented in the previous section. Donor doping creates n^+-type implantation on the backside of the detector, which helps to from contact between semiconductor and metal.

Diode structure in the detecting mode should be fully depleted by reverse bias voltage. Incident particles generate free charge carriers in the space charge region, which drift by applied electric field to the corresponding contacts. The holes drift to the node with negative potential and the electrons drift to the contact with positive potential. That process is illustrated in Figure 5.

The band gap of silicon E_g is 1.17 eV and it is indirect. Hence, to excite electrons from the valence band to the conduction band to create electron hole pair requires not only change in potential energy of electron but also change in momenta of the particle. This process excite phonons with specific energy to compensate the momentum changes. Therefore, at room temperatures minimum ionization energy for silicon detectors more than energy gap and equal 3.67 eV [10].

The minimum ionizing particles (MIP) could generate approximately 70 electron-hole pairs per micron in a fully depleted 300-μm-thick silicon. The average electric field of 10^4 V/cm cause electrons to drift through a 300-μm-thick semiconductor detector to positive contact approximately 10ns, and in that field holes are collected in approximately 25 ns [10]. The collection times of electrons and holes are connected with their mobilities, which determine charge carriers drift velocities respectively. Hence, as the mobilities of

charge carriers are temperature dependent: with decreasing temperature mobility increase. Thus, the drift velocities and measurements are also affected by the temperature.

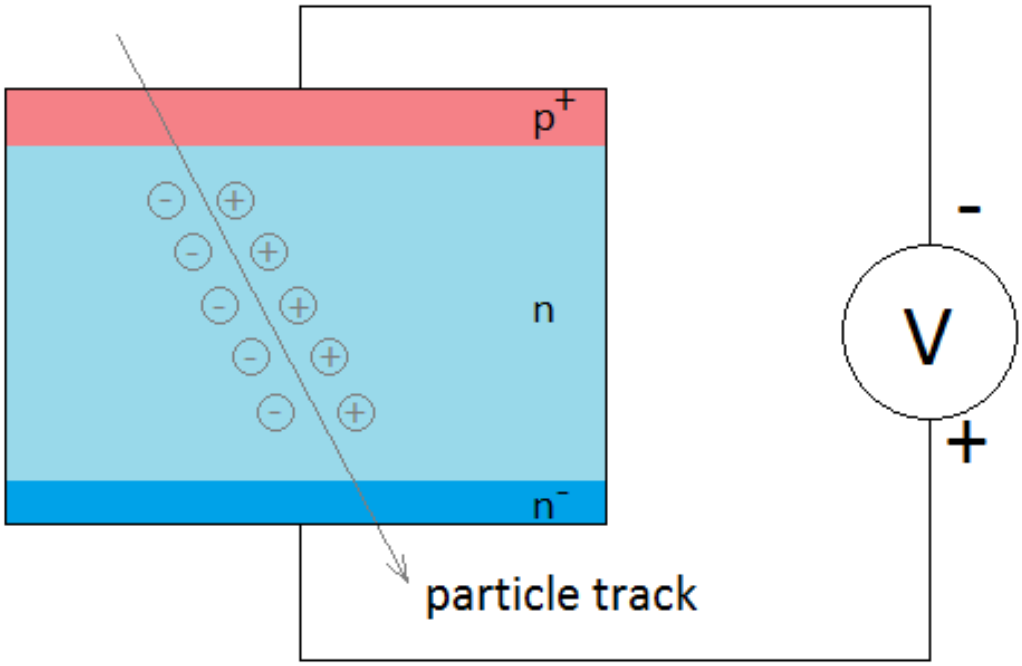

Figure 5: Operational principle of a fully depleted silicon particle detector.

3. TRANSIENT CURRENT TECHNIQUE MEASUREMENTS

The Transient Current Technique (TCT) measurements are based on principle to observe the signal of drifting free charge carriers in the silicon structure bulk, which are generated by laser light illumination on surface of the detector. When reverse bias voltage is applied to the silicon structure and front side of the detector is illuminated by red light, near this side in the structure bulk the process of creation free electrons and holes take place. One type of charge carriers with opposite sign to the front side node are collected faster by this contact. Free charge carriers with the same sign to the front side contact should go through the whole structure and get the backside contact. Current of those carriers is measured signal and called transient current. Figure 6 is illustrated two possible opportunities.

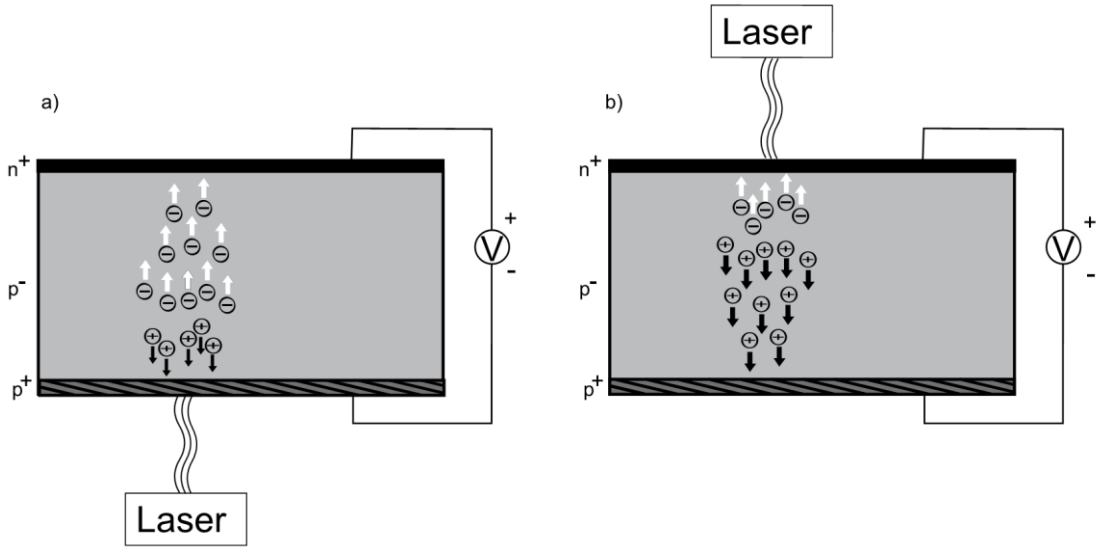

Figure 6: a) The resulting transient current is determined by electrons than the backside of a n^+-p^--p^+ diode is being illuminated. b) Illumination of the front side of the detector causes a TCT signal determined by holes [11].

The left figure shows the TCT signal generated by electrons in the case of illumination from the backside. On the other hand, the right figure illustrates current of holes in the bulk when light illuminate from the front side.

The Infrared laser generate photons, which could penetrate deeper into the 300-μm-thick silicon structure bulk. In this case, a TCT signal connected with both free charge carriers: electrons and holes, because generation process take place homogeneously in the whole detector bulk.

The TCT measurements based on diodes illuminated by infrared lasers give advantages in the determination of full depletion voltage V_{fd} and charge collection efficiency, because of reasons that were mentioned above. Moreover, if maximum of free electron and hole densities are generated near the electric filed maximum, the majority of charge carriers could be collected before the applied voltage reached V_{fd}.

3.1 Electric Field Distribution, Full Depletion Voltage and Effective Trapping Time Determination.

Electric filed applied to the detector determines the transient current in the structure. From the Ohm's Law:

$$\vec{\mathbf{J}} = \sigma\vec{\mathbf{E}} \tag{18}$$

where $\vec{J}$ is the current density at given location in the material, σ is a material dependent parameter called the conductivity, and $\vec{E}$ the electric filed at that location. In the TCT measurements the drift component of the current is dominant, hence the diffusion component depended on the carrier concentration in the bulk of semiconductor could be neglected. Therefore, Equation 18 could be rewritten for each type of charge carriers [9].

$$\mathbf{J}_n = q\mu_n n\mathbf{E} \tag{19}$$

$$\mathbf{J}_p = q\mu_p p\mathbf{E} \tag{20}$$

In equations 19 and 20 q is the elementary charge, n and p are concentrations of electrons and holes, and μ_n and μ_p are mobilities for corresponding type of that carriers.

Spatial configuration and location of the electric filed determines the shape of the transient current signal. The position of actual p-n junction sets the electric field maximum. Equations 19 and 20 show that drift current is proportional to the applied electric field; hence, the maximum of that current is highest at the location of junction, as well. The position of the p-n junction determines behavior of TCT signal. The shape of the TCT signal is descending, if the current is measured from the side near the p-n junction. In the case of detecting signal from the opposite side to the p-n junction, the behavior of the signal is ascending. Figure 7 shows two possible variants of behavior of transient current signal.

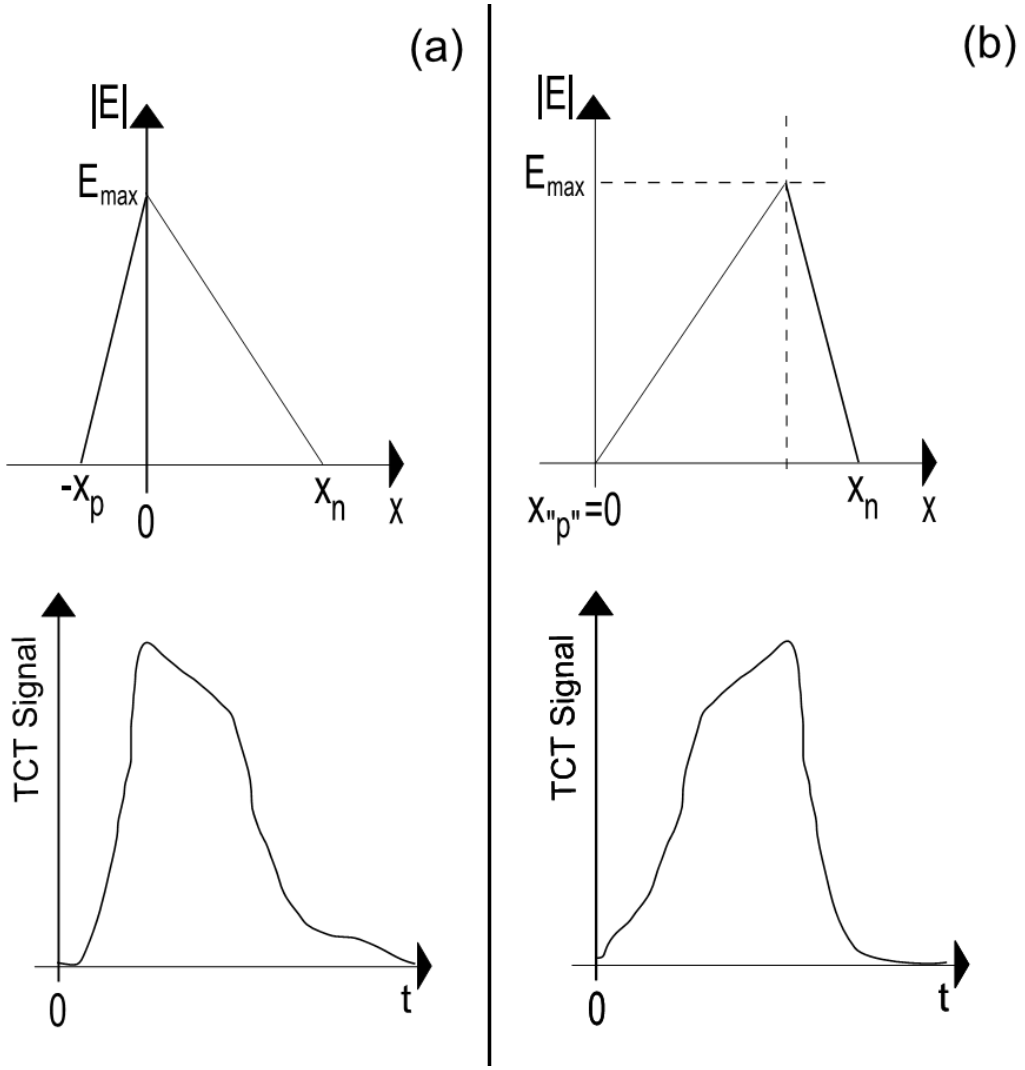

Figure 7: a) A p^+-n-n^+ silicon detector with the p-n junction near the front side provides the electric filed maximum at that side and descending TCT signal. b) A p^+-n-n^+ structure determines the electric filed maximum at the backside of the detector and ascending shape of TCT signal [11].

From the TCT measurements one could obtain the full depletion voltage V_{fd} and the effective trapping time τ_{eff}. In addition, the collected charge could be extracted from the transient current by integration the TCT signal over time.

The process of charge collection increases until the applied voltage reaches V_{fd} where that process starts saturates. Possible way to obtain the full depletion voltage V_{fd} is to find intersection of two linear fittings at the graph of the collected charge depending on bias voltage, as it is shown on figure 8.

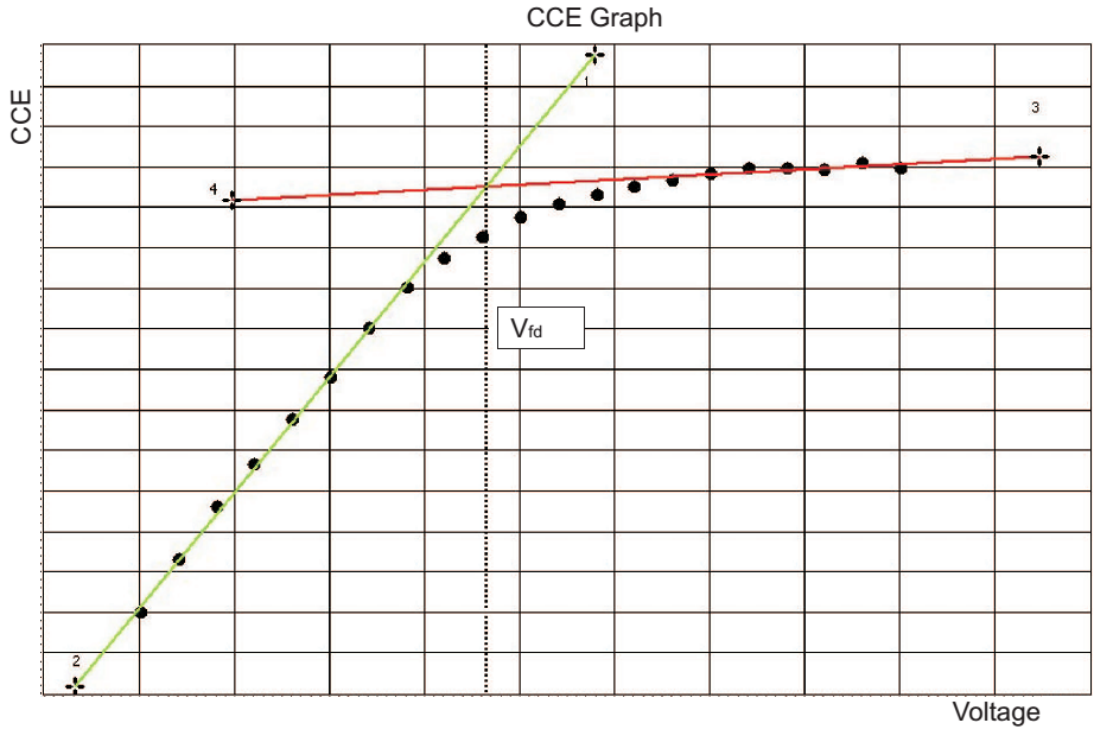

Figure 8: Graphical way of determination V_{fd} from the charge collection efficiency plot. Green and red lines are linear fittings of CCE graph [11].

Ramo's theorem [12] determines connection between transient current and charge carrier, which cause that current.

$$i(t) = q v_{dr} \mathbf{E}_v = q\mu E(x) \frac{1}{D} \tag{21}$$

Charge carrier q with the velocity v_{dr} creates in its location unit potential, which determines electric filed $\mathbf{E}_v$. In the right hand side of the equation 21 v_{dr} is replaced by carrier mobility μ and electric filed $E(x)$. D is the value of diode thickness. To obtain the full transient current $I(t)$, the transient current caused by one charge carrier $i(t)$ should be multiplied by the carrier concentration n. In turn, the carrier concentration depends on effective trapping time τ_{eff} [13]. That dependence could be written as:

$$n = n_0 \cdot e^{-\frac{t_{dr}}{t_{eff}}} \tag{22}$$

where n_0 is the injected carrier density, t_{dr} is the drift time of the injected carriers through the whole structure. The equation 22 shows that electron concentration decreases depending on effective trapping time. According to previous equations, the total transient current results in:

$$I(t) = n_0 \frac{q\mu E(x)}{D} e^{-\frac{t_{dr}}{t_{eff}}} \tag{23}$$

Equations 23 for total transient current, but without exponential correction connected with trapping, equals the current that can be received from the equations 19 and 20 for current density (Ohm's law).

Integration the total transient current over the time helps to obtain the collected charge.

$$\begin{aligned} Q &= \int_0^{t_{dr}} I(t)dt = \\ &= \frac{Q_0 v_{dr}}{D} \int_0^{t_{dr}} e^{-\frac{t}{t_{eff}}} dt \\ &= \frac{Q_0 v_{dr}}{D} \tau_{eff} \left(1 - e^{-\frac{t_{dr}}{t_{eff}}}\right) \\ &= \frac{Q_0 W}{D} \frac{\tau_{eff}}{t_{dr}} \left(1 - e^{-\frac{t_{dr}}{t_{eff}}}\right) \end{aligned} \tag{24}$$

In this formula, it was guessed that the electric filed through the diode is constant and, hence, it means that there is no dependence from the position *x*. In this equation $v_{dr}\tau_{eff}$ could be replaced by *W*. The charge collection efficiency (CCE) can be obtained from the final formula of equation 24 dividing that by Q_0.

$$CCE = \frac{Q}{Q_0} = CCE_g \cdot CCE_t = \frac{W}{D} \frac{\tau_{eff}}{t_{dr}} \left(1 - e^{-\frac{t_{dr}}{t_{eff}}}\right) \tag{25}$$

When the depletion width *W* equals the diode thickness *D*, the CCE is determined only by τ_{eff}. In this case, for bias voltages more than V_{fd} the amount of collected charge is permanent. The final result of equation 24 could be used for calculation the effective trapping time τ_{eff} by determining the collected charge Q, which could be obtained by integration the measured transient current over the time.

3.2 Transient current technique measurement setup

Measurement setup presented in this thesis and simulated in TCAD Mixed Mode Simulator based on TCT measurement setup designed by CERN RD39 Collaboration [14]. This setup is an effective research instrument to explore heavy irradiated silicon detectors. The TCT method was suggested and verified by Ioffe Institute and the Brookhaven National Laboratory [15, 16]. There is possible way to obtain the full depletion voltage, effective trapping time, electric field distribution and the sign of the space charge in the silicon bulk. An overview of the real CERN RD39 Collaboration measurement setup is presented in figure 9 [17].

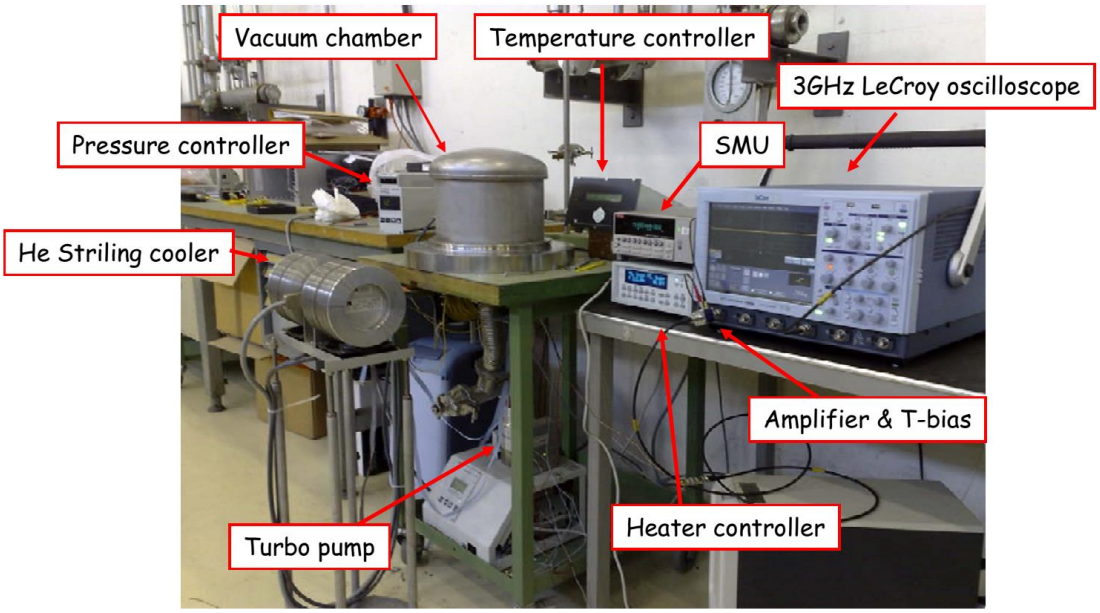

Figure 9. Transient current technique measurement setup [16].

The TCT setup consists of a Tektronix TDS 784C 1 GHz bandwidth oscilloscope, a Keithley 6487 source meter unit, vacuum chamber, cold finger, Leybold helium cooler, temperature and vacuum control units. The system has two lasers emitting 678 and 1060 nm light. Red laser helps to obtain information about the space charge. Infrared laser illumination generates electron-hole pairs homogenously through the entire silicon bulk. The duration of the laser pulse is about 30ps and the maximum optical power is 250 mW [14]. A schematic overview of the TCT setup is shown in figure 10.

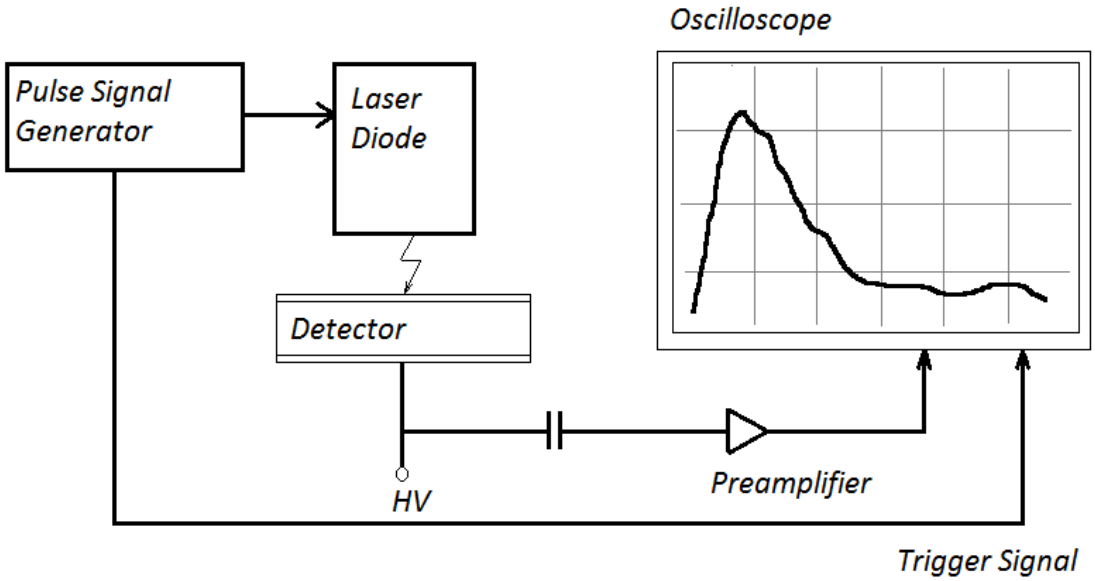

Figure 10. Schematic view of transient current technique measurement setup.

4. SIMULATION SOFTWARE

The research in the field of semiconductor physics requires great theoretical work, but the next step should be an experiment. Often great amount of money is needed to do the experiment or the final device. That is why often the theory or new devices are tested using modeling software. One of the companies specializing in software for modeling and simulation of semiconductor devises is Silvaco International.

Silvaco provides Technology Computer Aided Design (TCAD) process and devices simulation software. This framework includes many tools research in semiconductor field. The devise structure is defined in a special mesh file, which could be created in DevEdit (Structure and mesh editor) or ATHENA (Process Simulator). The core tool that is used for device simulation is ATLAS. This tool needs direct-input command file created in DeckBuild. In this research MixedMode circuit simulator and Luminous 2D optoelectronics device simulator are used. The command file written in DeckBuild allows creating mesh or loading structure file of the detector. Than it allows to create a circuit using MixedMode simulator and illuminate device using Luminous tool. ATLAS creates log files and solution files, which could be visualized in TonyPlot. Scheme of inputs and outputs of ATLAS is shown in figure 11.

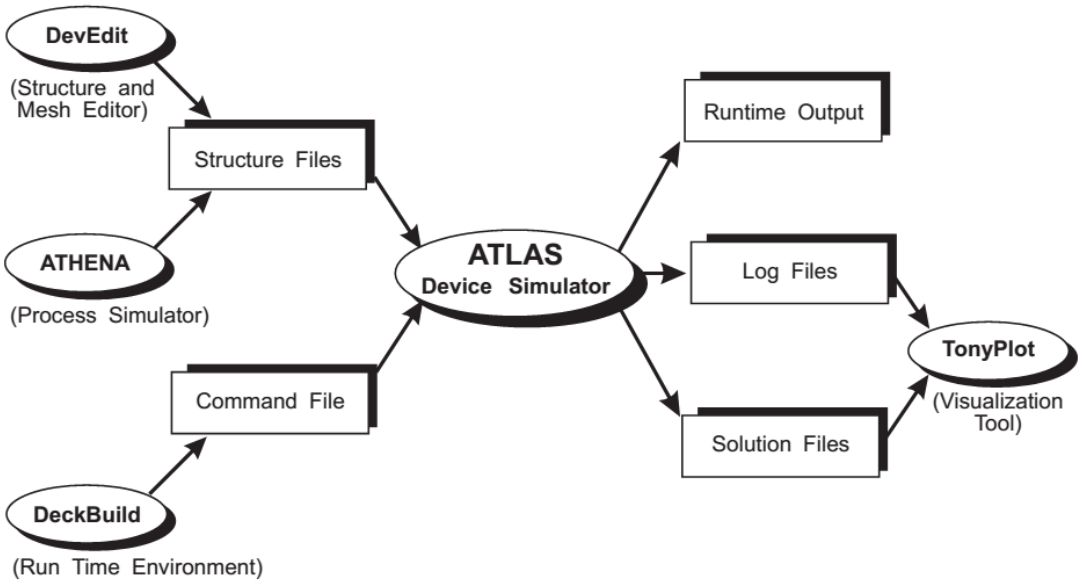

Figure 11. ATLAS inputs and outputs [18].

Main steps for simulation structures in ATLAS are described in the following paragraph. The first step is mesh description that is presented in figure 12. There are number of triangles, which are important for simulation accuracy. On the other hand, their number influence simulator execution time that is why it is important to find a balanced value. High concentration of triangles are needed near junctions or material boundaries. It is good way to obtain results that are more accurate and do not take much computation time.

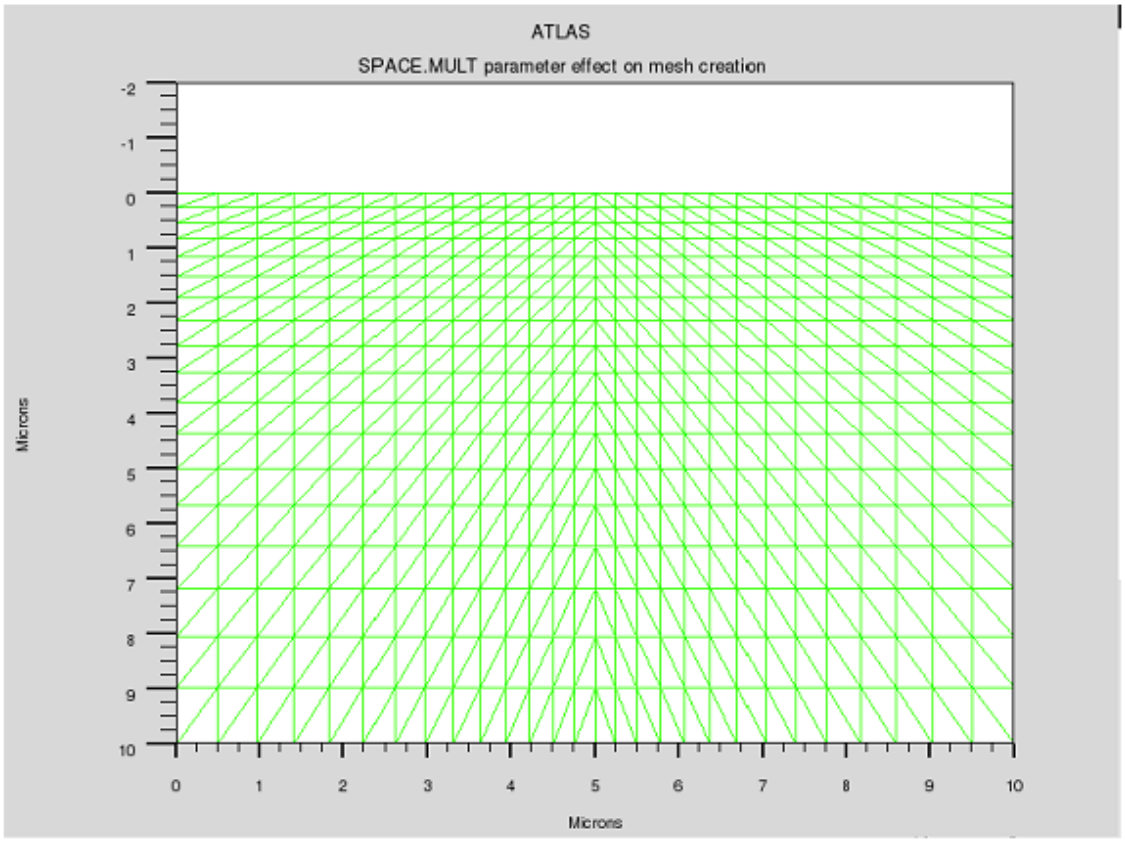

Figure 12. Mesh of the structure build in ATLAS software [18].

After mesh definition the material regions should be specified. That regions could be doped by acceptor or donor dopant. It could be done in a regular uniform way, in linear or Gaussian distribution. The example of that is shown in figure 13. The next step is definition of electrodes. Their position, size and material should be specified.

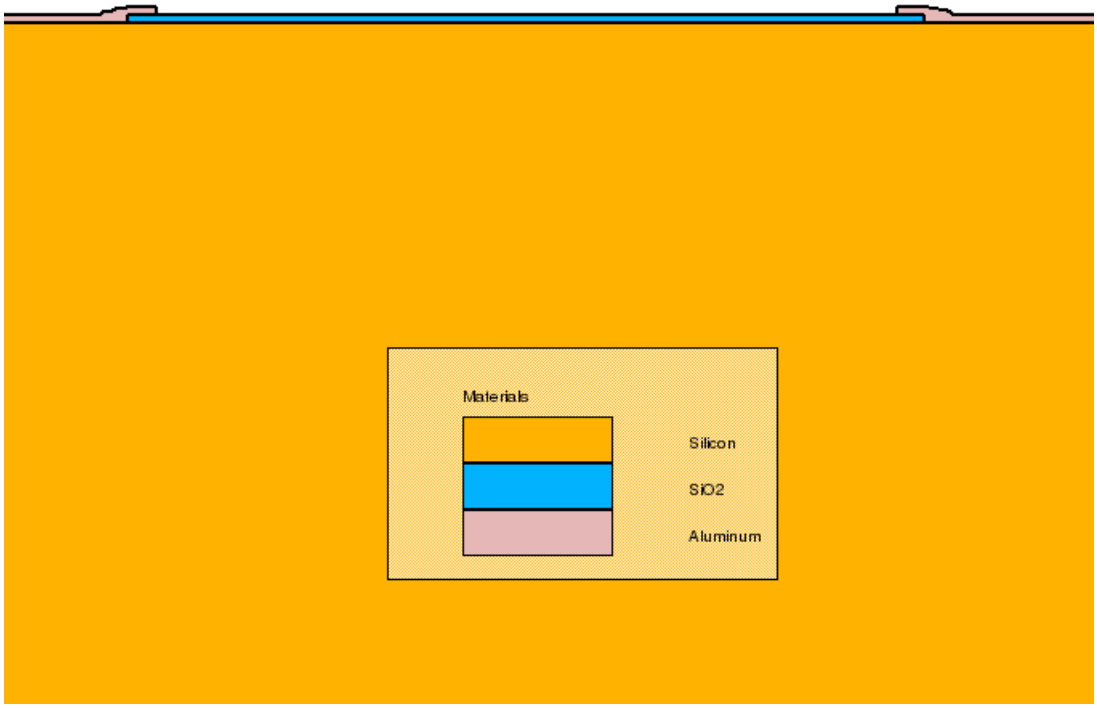

Figure 12. Structure with specified regions.

After mesh and material definition, specification of contacts the structure is ready for simulation. Simulated device could be applied bias voltage or illuminated.

4.1 Mathematical models used in ATLAS.

Years of investigation of semiconductors and solid-state materials have resulted in creation of mathematical model of their physics. There are set of fundamental equations that operates in any semiconductor material [9]. These formulas derived from Maxwell's laws describe connections between the electrostatic potential and the carrier densities. This mathematical model include Poisson's equation, the continuity equations and the transport equations. All these equations are solved in any general-purpose device simulation software.

Connection between the electrostatic potential and space charge density is described in Poisson's equation:

$$div(\varepsilon \nabla \varphi) = -\rho \qquad (26)$$

where φ is the electrostatic potential; ρ is the local space charge density and ε is the local permittivity. The local space charge density is determined by the sum of all mobile (electrons, holes) and fixed charges (ionized impurities).

The continuity equations for electrons and holes are defined by next equations.

$$\frac{dn}{dt} = \frac{1}{q} div\overrightarrow{J_n} + G_n - R_n \quad (27)$$

$$\frac{dp}{dt} = -\frac{1}{q} div\overrightarrow{J_p} + G_p - R_p \quad (28)$$

where n and p are electron and hole concentrations; J_n and J_p are the electron and hole current densities; G_n and G_p are the generation rates for electrons and holes; R_n and R_p are the recombination rates for electrons and holes; q is the elementary charge.

Drift-Diffusion Model is the simplest model of charge transport. That model is adequate for calculation for most devices. Nevertheless, it becomes less accurate for submicron devises. The energy balance and hydrodynamic models give better results in this case. The current densities in Drift-Diffusion Model are defined as:

$$\overrightarrow{J_n} = q\mu_n n\overrightarrow{E_n} + qD_n\nabla n \quad (29)$$

$$\overrightarrow{J_p} = q\mu_p p\overrightarrow{E_{np}} + qD_p\nabla p \quad (30)$$

where μ_n and μ_p are the electron and hole mobilities; $D_n$and D_p are diffusion coefficients for electrons and holes.

5. SIMULATION AND RESULTS

The main idea of any simulation is to create model, which will be adequate to predict behavior of the real device. It is used for more clarify understanding of device operation principles and for modification of existing device structures.

5.1 Mixed Mode: Mixed Circuit and Device Simulator

One of the main objective of this work was to understand operation of MixedMode tool in TCAD framework. In this chapter MixedMode tool is described and basic circuit is simulated.

MixedMode is a circuit simulator that can include elements simulated using device simulation and compact circuit models. It combines different levels of abstraction to simulate relatively small circuits where compact models for single devices are unavailable or sufficiently accurate. MixedMode also allows you to also do multi-device simulations. MixedMode uses advanced numerical algorithms that are efficient and robust for DC, transient, small signal AC and small signal network analysis.

MixedMode is typically used to simulate circuits that contain semiconductor devices for accurate compact models that do not exist or circuits where devices play a critical role must be modeled accurately. MixedMode circuits can include up to 200 nodes, 300 elements, and up to ten numerical simulated Atlas devices. The circuit elements that are supported include dependent and independent voltage and current sources as well as resistors, capacitors, inductors, coupled inductors, MOSFETs, BJTs, diodes, and switches. Commonly used SPICE compact models are available. The SPICE input language is used for circuit specification [18].

Basic circuit presented in figure 13 is simulated first. It is consists of resistor, diode and bias voltage source. Moreover, there is a optical source that has wavelength 623 nm. DeckBuild program described this circuit could be found in Appendix 1. The circuit has three nodes. They are numbered from 0 to 2 and shown in figure 13. Using these points, elements of the circuit could be connect with each other. It is simply to specify this circuit using SPICE format. Optical source generates 10 ns rectangular shape pulse of light. The detector is illuminated from the bottom side where cathode is situated. Part of the photodiode in area of front view is shown in figure 14.

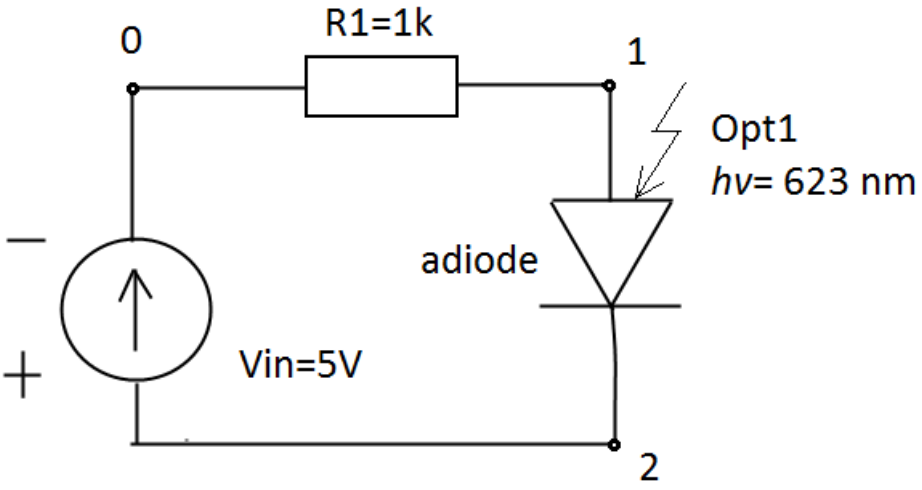

Figure 13. The scheme of simulated circuit

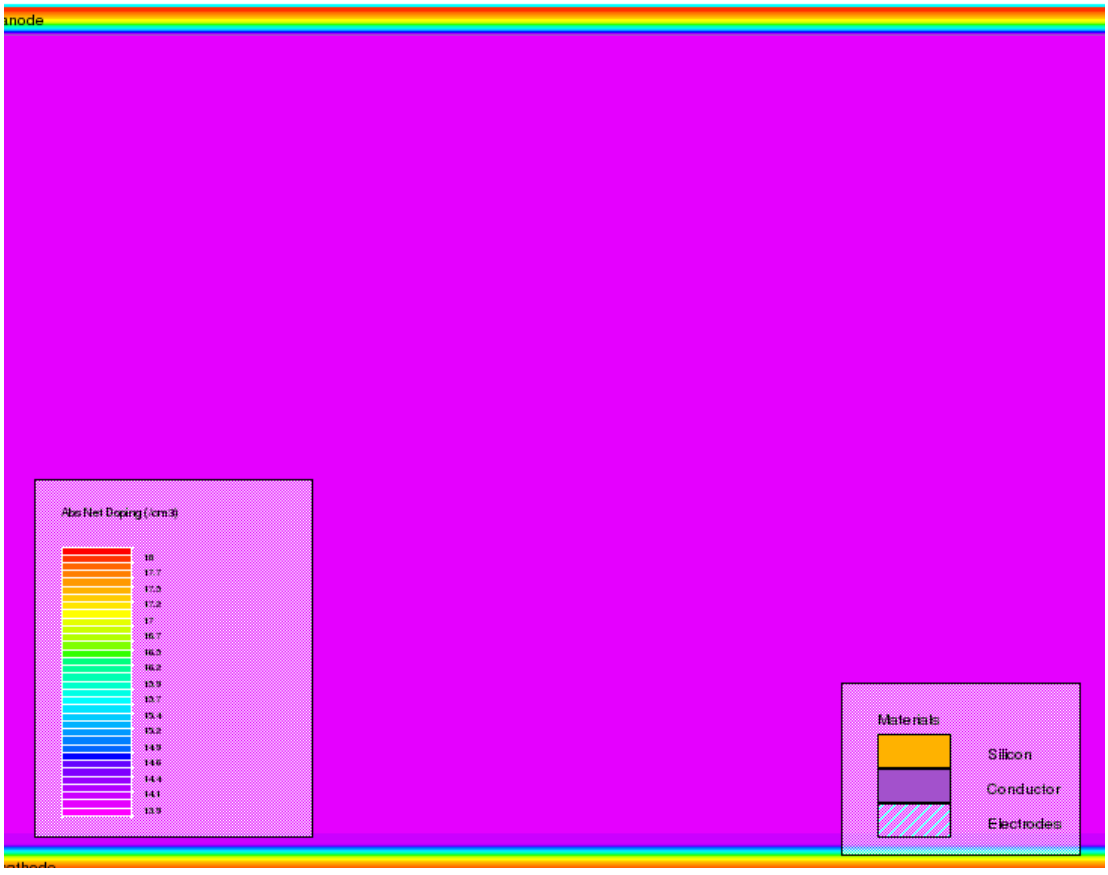

Figure 14. Photodiode in front view

Results of simulation are presented in figures 15-17. Figure 15 shows available photo current (red line) that has the same rectangular shape as optical impulse. The impulse of that current changes from zero to it is maximum value that is equal 0.5 mA.

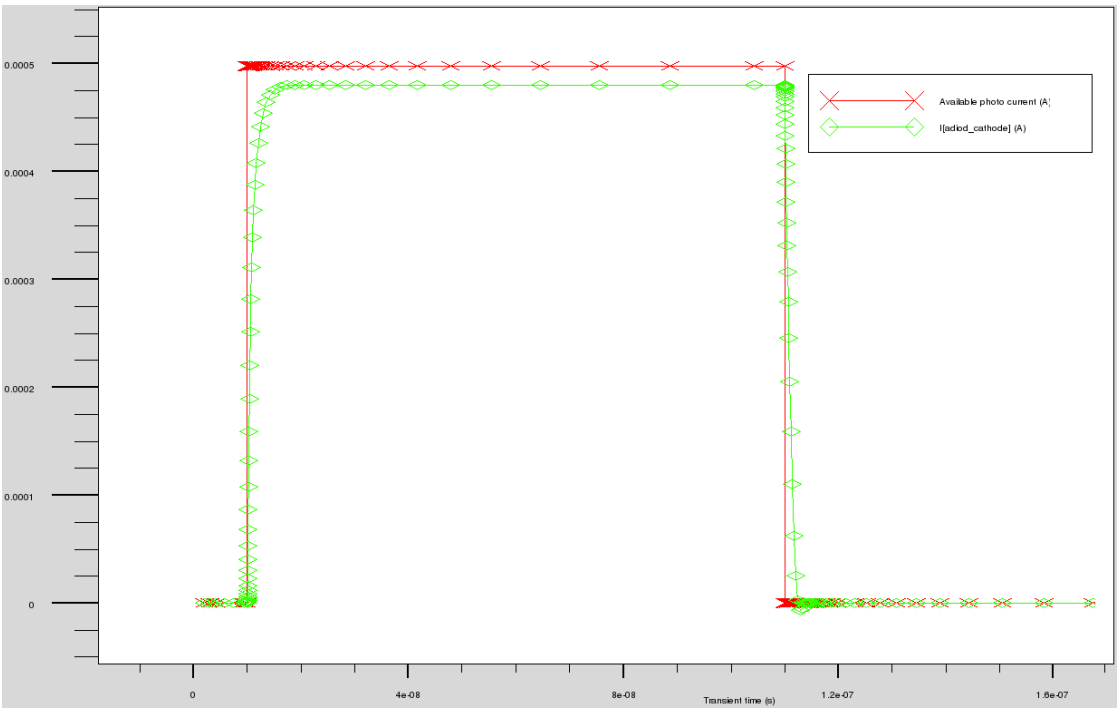

Figure 15. Measured currents. Red line – available photo current; Green line – cathode current.

On the other hand, cathode current behaved differently. When illumination is turn on, it starts growth, but not so abruptly as the available photocurrent. Cathode current reaches its maximum value 0.48 mA after proprocession of 7ns. Whereupon that process starts saturates. Zoomed part of that process is presented in figure 16. Cathode current in this case is connected with generation process, which can not reach it maximum value immediately after the lighting. That process determines the behavior of the green curve.

After illumination is turned off available photo current changes abruptly from 0.5mA to zero. As in the previous case, curve of cathode current changes more smoothly. It takes 4 ns for that current to decrease from 0.48 mA to zero amperes. Zoomed graphic of the process is shown in figure 17. Moreover, region with negative cathode current can be seen in the figure 17. When illumination is stopped, cathode current is determined by recombination process.

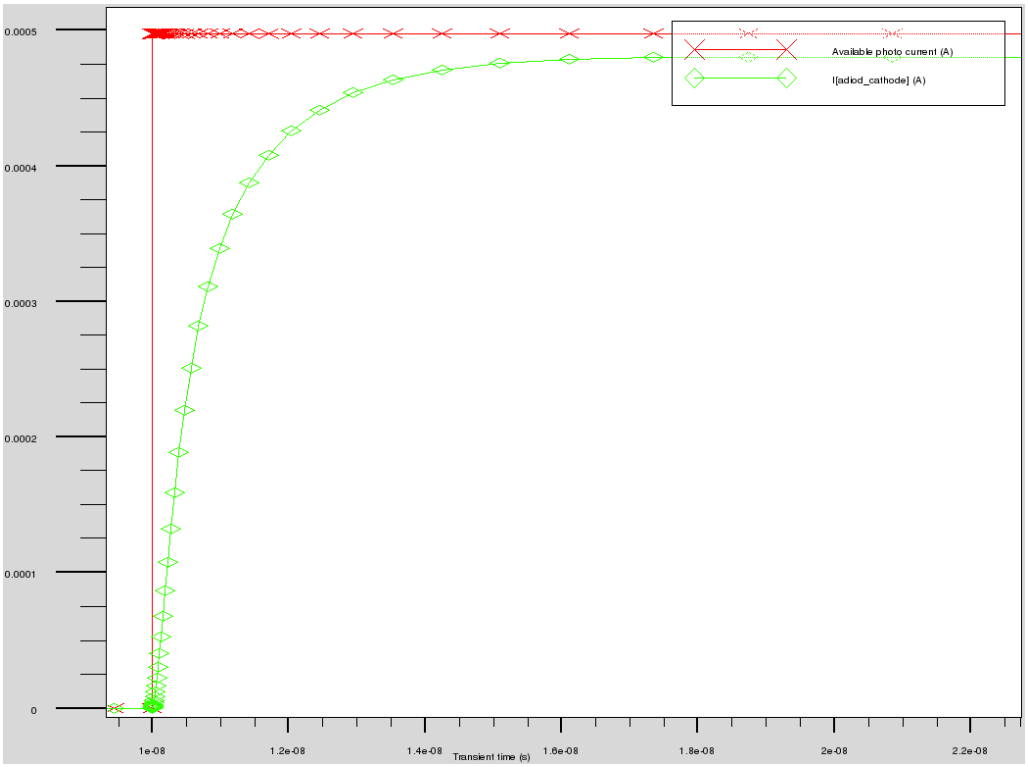

Figure 16. Zoomed part of graphics of the moment when illumination is started.

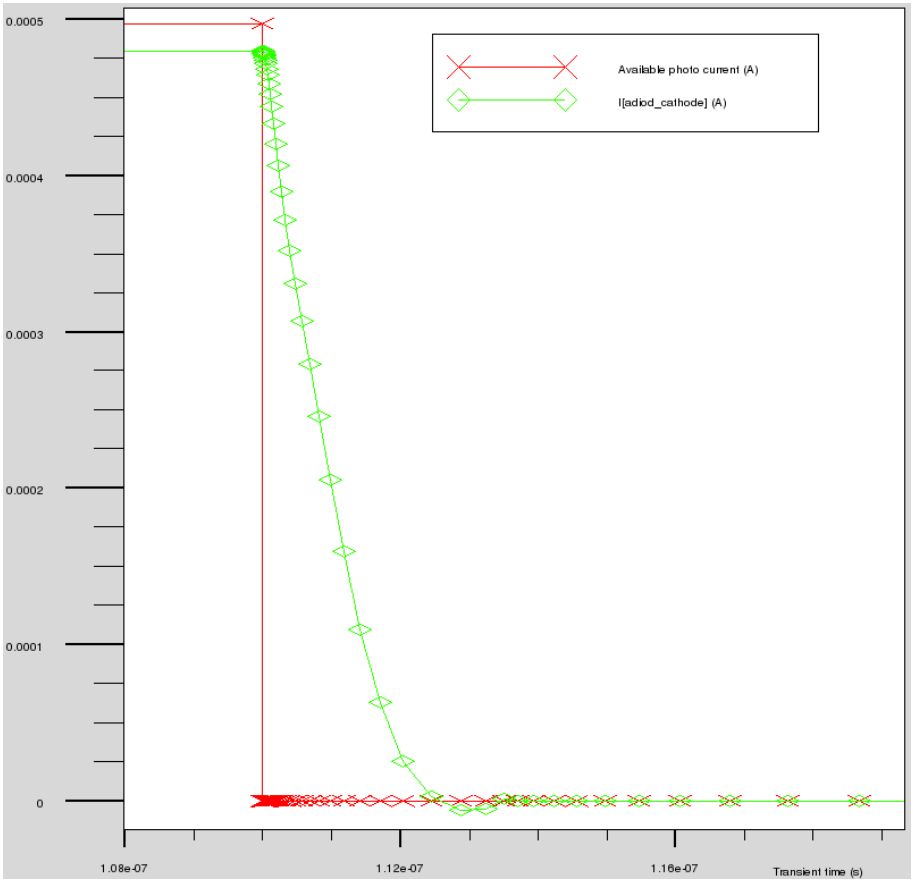

Figure 17. Zoomed part of graphics of the moment when illumination is stopped.

5.2 Mixed Mode simulation of new p-type strip detectors

Silicon strip detectors were the first devices using the lithographic capabilities of microelectronics to produce a detector with high position resolution. A strip detector is an arrangement of strip like shaped implants acting as charge collecting electrodes. Placed on a low doped fully depleted silicon wafer these implants form a one-dimensional array of diodes. By connecting each of the metalized strips to a charge sensitive amplifier a position sensitive detector is built. Two dimensional position measurements can be achieved by applying an additional strip like doping on the wafer backside by use of a double sided technology.

Strip detectors fabricated with a N on P technology show a number of advantages for many applications over other detectors fabricated with a P on N or N on N technologies [19–21]. The collection of electrons instead of holes provides a faster response with a lower trapping probability. Besides, p-type substrates do not undergo inversion, allowing highly efficient operation even under incomplete depletion conditions[22].

In spite of their good features, irradiated silicon strip detectors suffer displacement damage that changes their charge collection properties. The mechanisms that alter the behavior of the detectors have been identified as defect levels in the forbidden gap [23]. These defect levels introduce noticeable trapping of the signal charge carrier that greatly reduces the collected charge [24]. Nonetheless, a higher signal than expected from the model of the charge trapping on the irradiation fluence has been reported [25]. This effect is macroscopically expressed as a multiplication in the collected signal. The multiplication effect is not found in non-irradiated silicon detectors, indicating that the radiation induced defects cause a change in the effective space charge that leads to an increase of the electric field at the junction between the N^+ electrode and the p-type substrate. This electric field increase a multiplication of the collected charge due to the impact ionisation mechanism [22].

The conventional p-type strip detector structure, showed in Figure 18. Typically, this conventional detector configuration consists in a series of N^+ strips on a highly resistive p-type substrate. Under reverse bias voltage, the very lowly doped P^- side of the abrupt N^+ /P^- junction is rapidly depleted. A high electric field value is then establishing throughout the substrate, allowing the drift collection of the generated electron-hole pairs.

The surface of the low doped substrate is inverted due to the positive charge existing in the SiO_2 and the Si/SiO_2 interface. In order to avoid the short-circuit between the strips, a p-type doped diffusion is placed between the pitches [22].

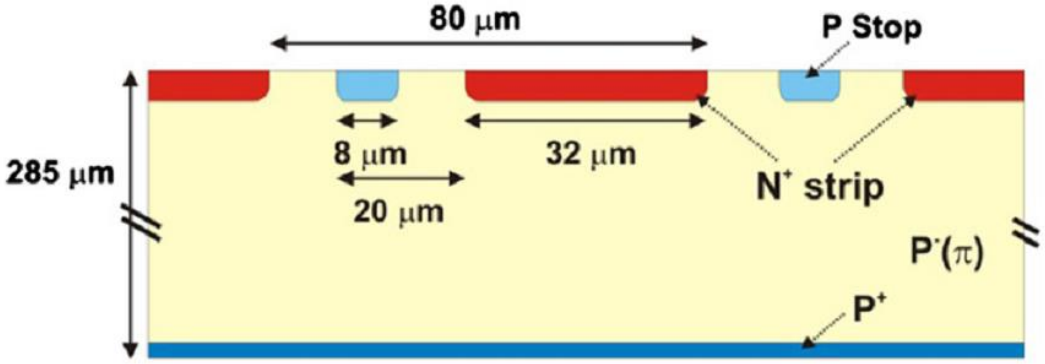

Figure 18. Schematic view of the structure of conventional p-type stripped detector [24]

The structures studied in this work have been simulated with the aid of the Silvaco TCAD-physic based simulation framework. The simulations have been made using a simplified 2D model considering only one strip and the two half strips at the neighborhood, to avoid false boundary effects. The model of strip detector was made by Anatolii Dementev. Deckbuild code of that detector could be found in Appendix 2. An area factor of 1 cm has also been chosen to reproduce the third dimension. Doping dependent models for the mobility and SRH recombination have been considered, impact ionization process was also taken into account. Figures 19 and 20 show view of 2D and 1D doping profiles of the structure of conventional p-type stripped detector simulated in TCAD. Zoomed area of cathode of that detector are presented in figures 21-22. Zoomed 2D area of the electric field distribution in conventional p-type strip detector under 600 V reverse voltage bias is shown in figure 23 and electric field profile along a cross-section at the center of the detector is presented in figure 24.

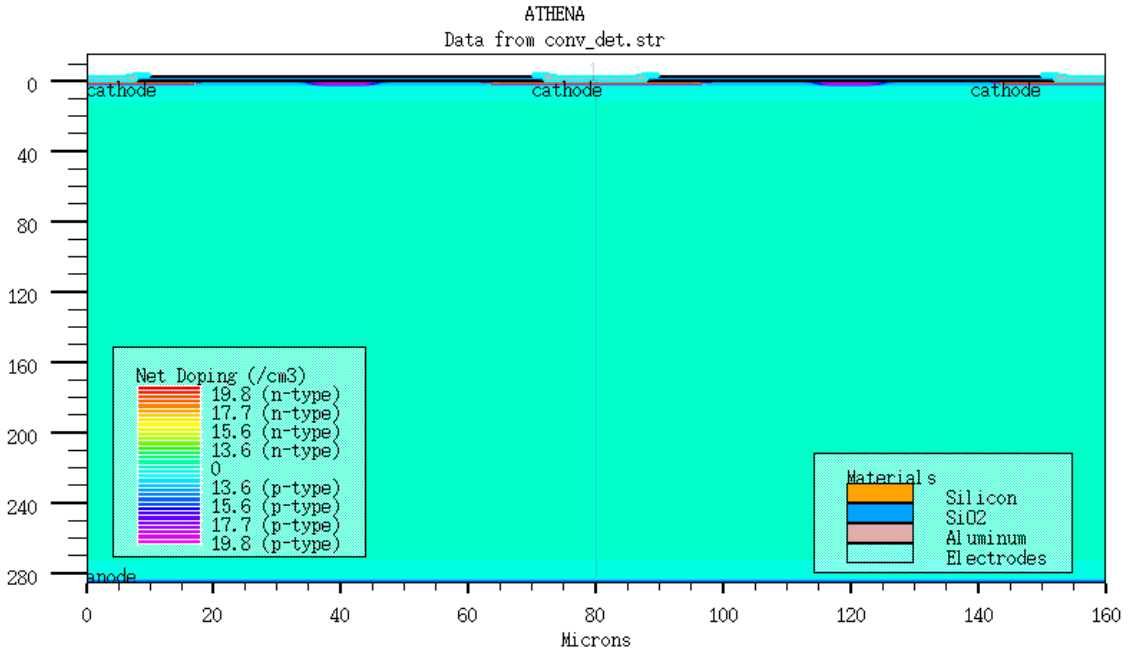

Figure 19. View of the structure of conventional p-type stripped detector simulated in TCAD.

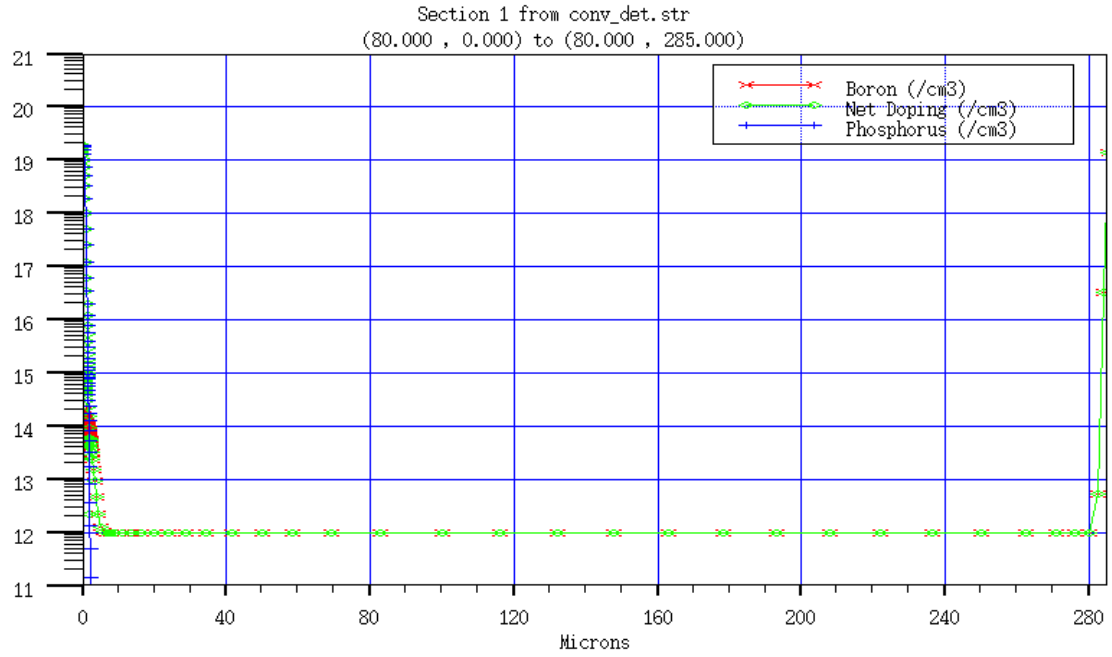

Figure 20. 1D doping profile of simulated conventional p-type stripped detector

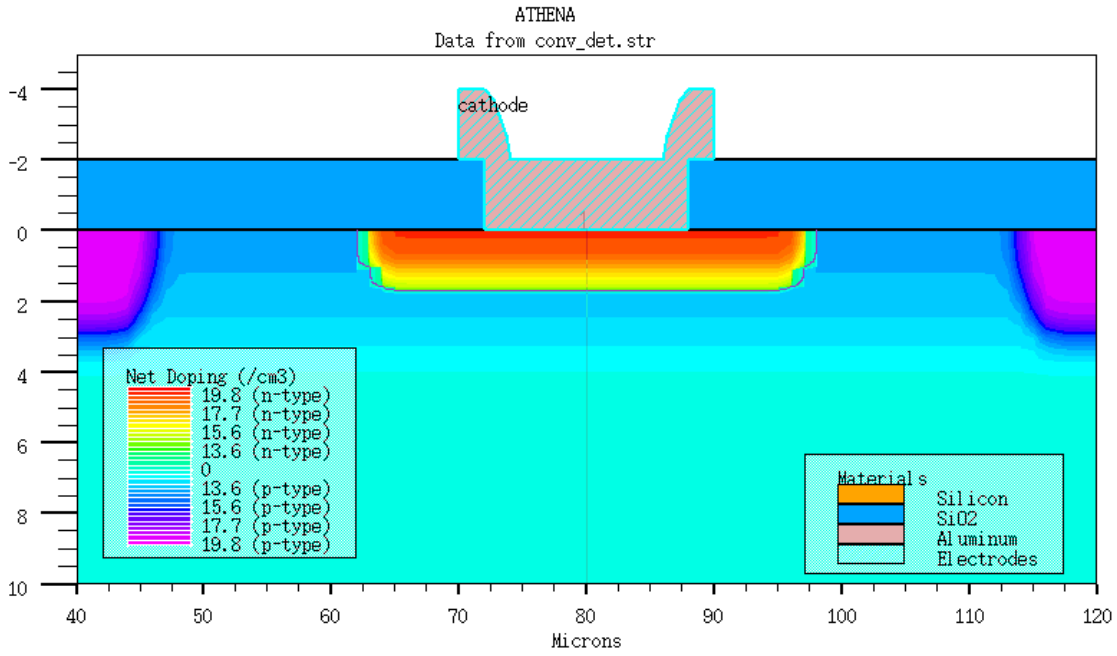

Figure 21. Zoomed view of 2D doping profile of conventional p-type stripped detector simulated in TCAD.

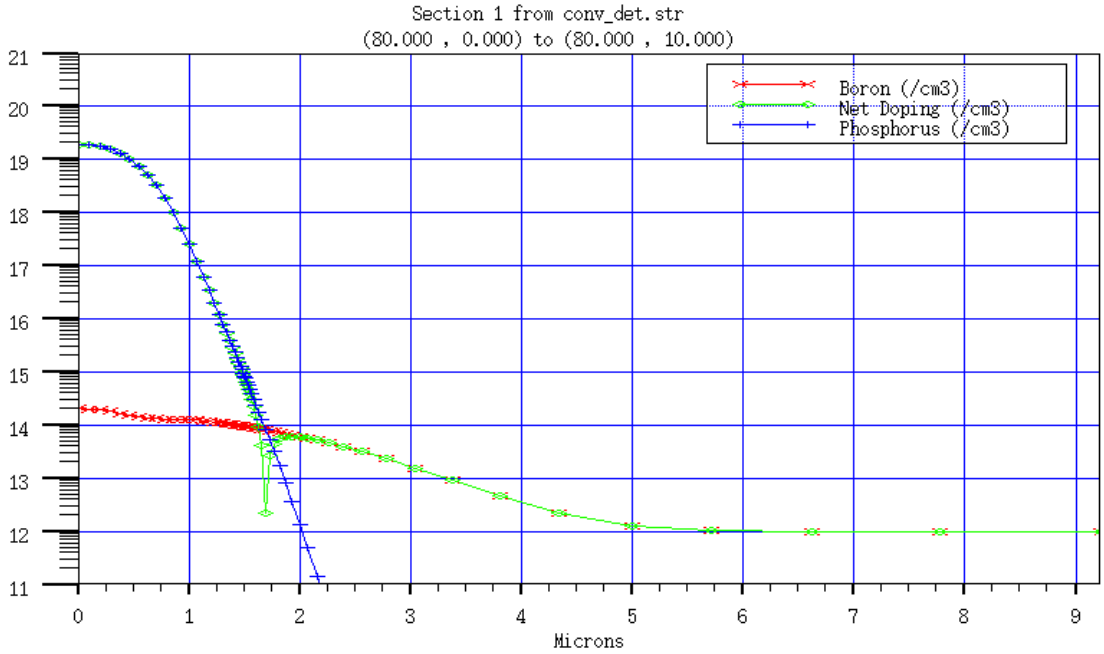

Figure 22. Zoomed view of 1D doping profile of simulated conventional p-type stripped detector

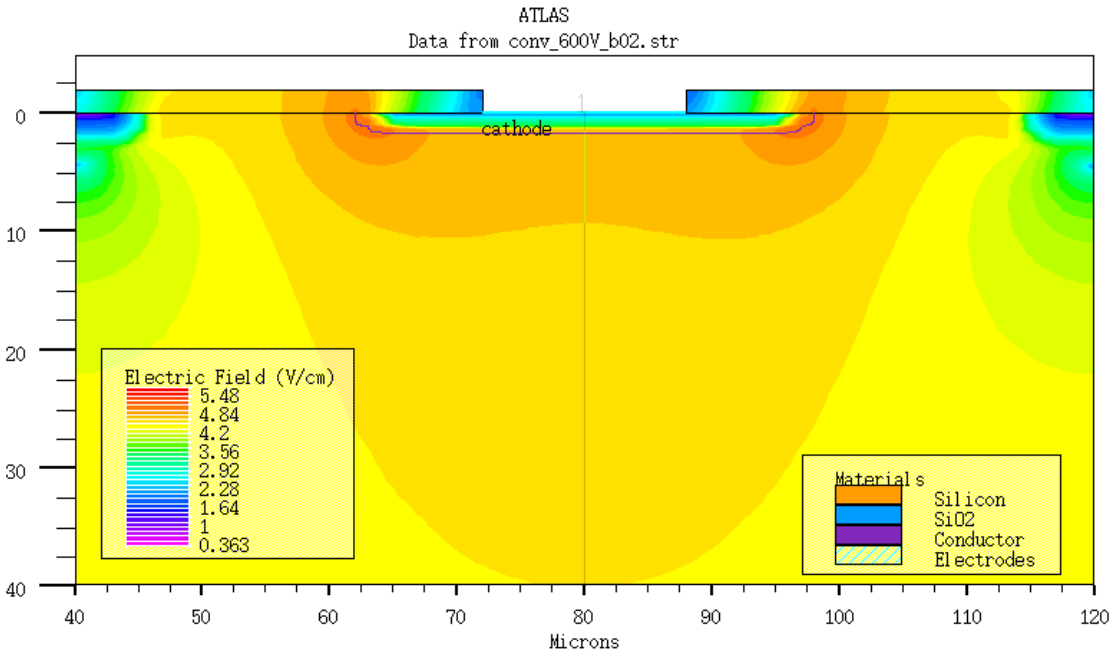

Figure 23. Simulated electric field distribution in conventional p-type strip detector at an applied reverse voltage of 600 V.

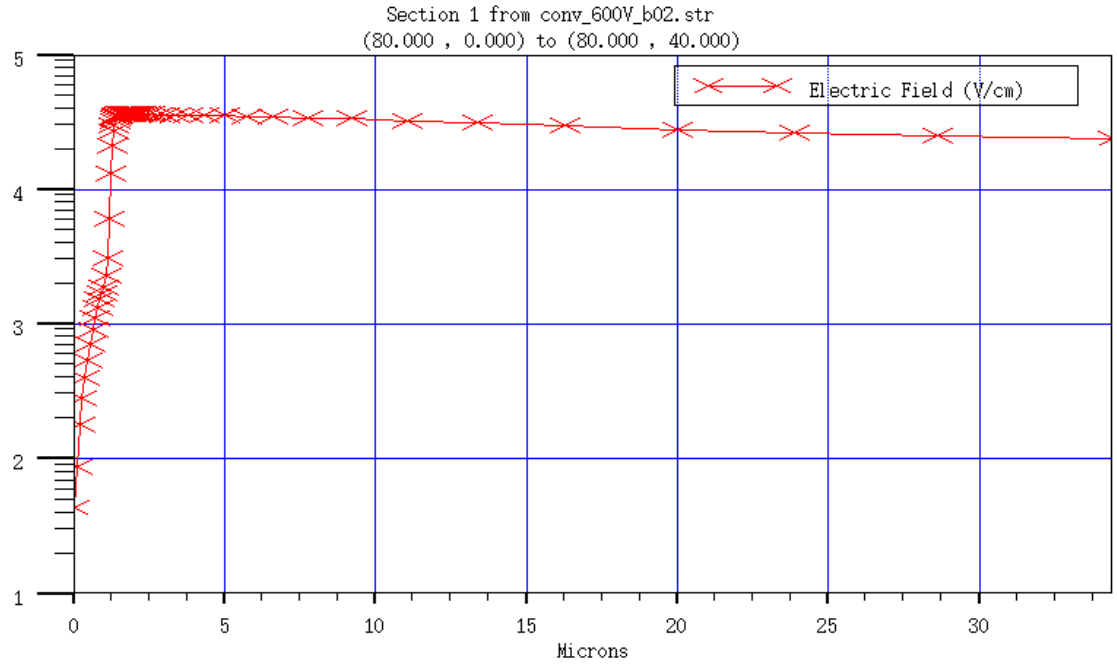

Figure 24. Simulated electric field profile along a cross-section at the center of the detector

Transient current measurements of conventional p-type strip detector at an applied reverse voltage of 600 V is made using structure presented in previous paragraphs and measurement setup shown in chapter 5.1. The detector is illuminated by laser light with wavelength 623 nm and pulse width 10 ns. Optical source has extremely small pulse edges about 1 ps. It means that in this simulation ideal rectangular optical impulse is used. Transient current caused by that optical source is presented in figure 25. The shape of optical impulse could be defined using available photocurrent.

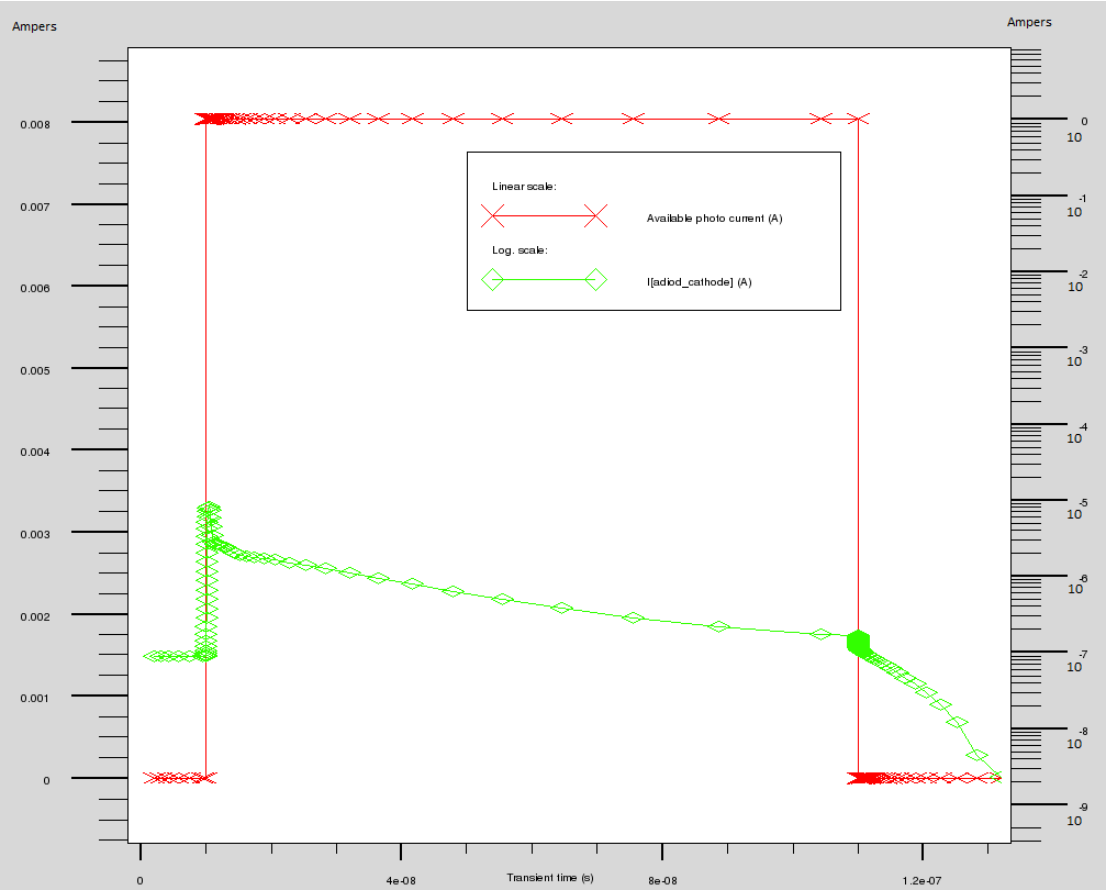

Figure 25. Available photocurrent (red line) and TCT current (green line). Detector under reverse voltage bias 600 V and optical power 1 W/cm^2.

When illumination is turned on, cathode current begins to rise sharply. However, after reaching maximum value of that current it starts to decrease smoothly. The rate of decrease increases when illumination is stopped. Zoomed areas near optical pulse leading edge and pulse trailing edge are shown in figures 26 and 27.

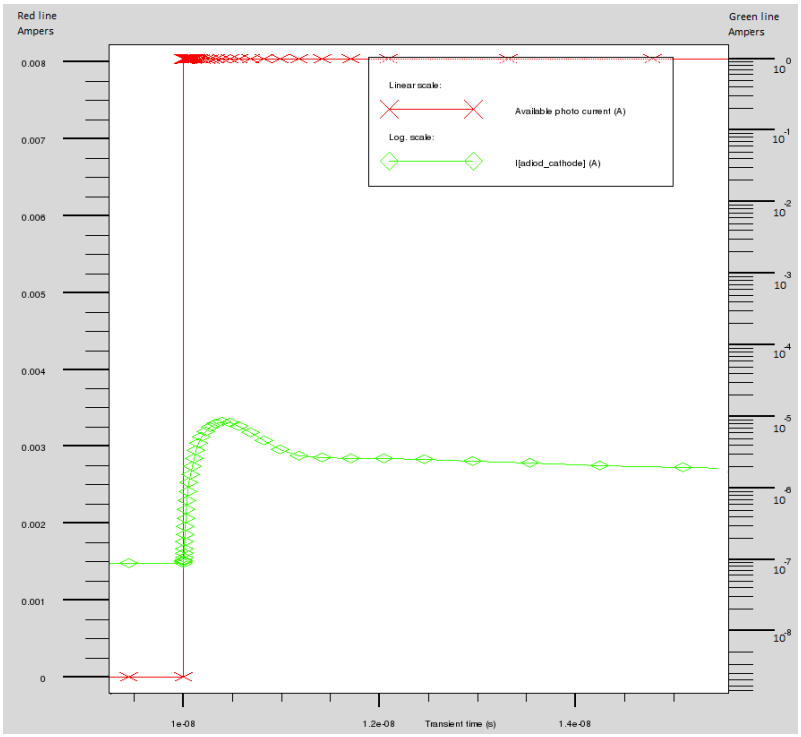

Figure 26. Zoomed area of pulse leading edge. Red line – available photocurrent; green line – cathode current.

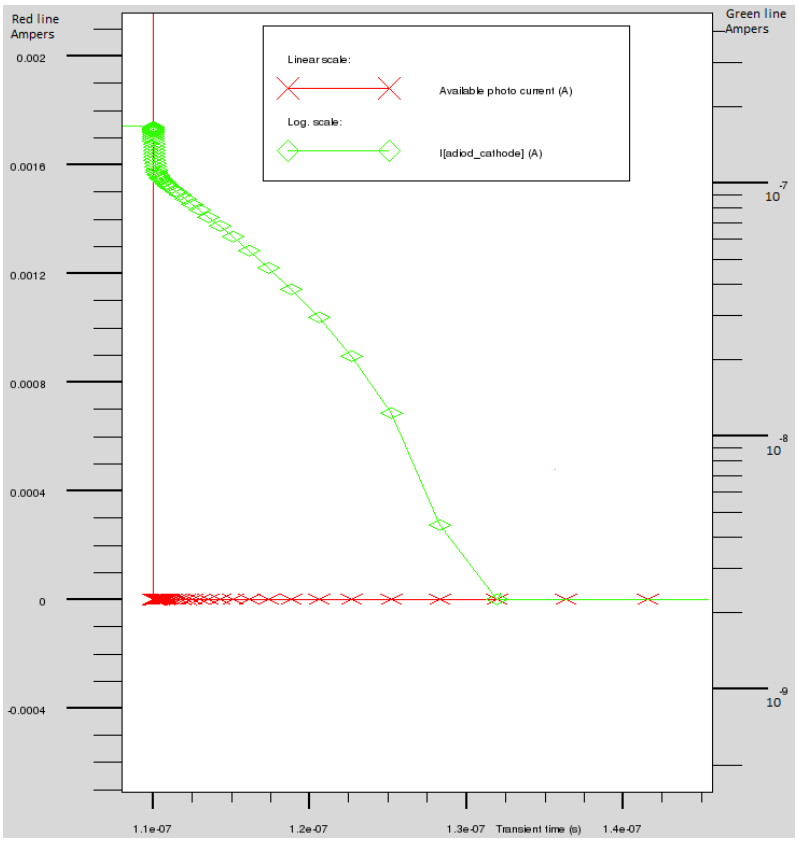

Figure 27. Zoomed area of pulse trailing edge. Red line – available photocurrent; green line – cathode current.

In the case of decreasing optical impulse width, the graphics presented in the following figure could be obtained. It shows TCT signal defined by 10 ps illumination pulse. Detector under reverse voltage bias 600 V and optical power 1 W/cm^2. The shape of the signal is similar to the shape of TCT signal in figure 7a. Physics describes the shape of TCT signal is presented in Chapter 3.

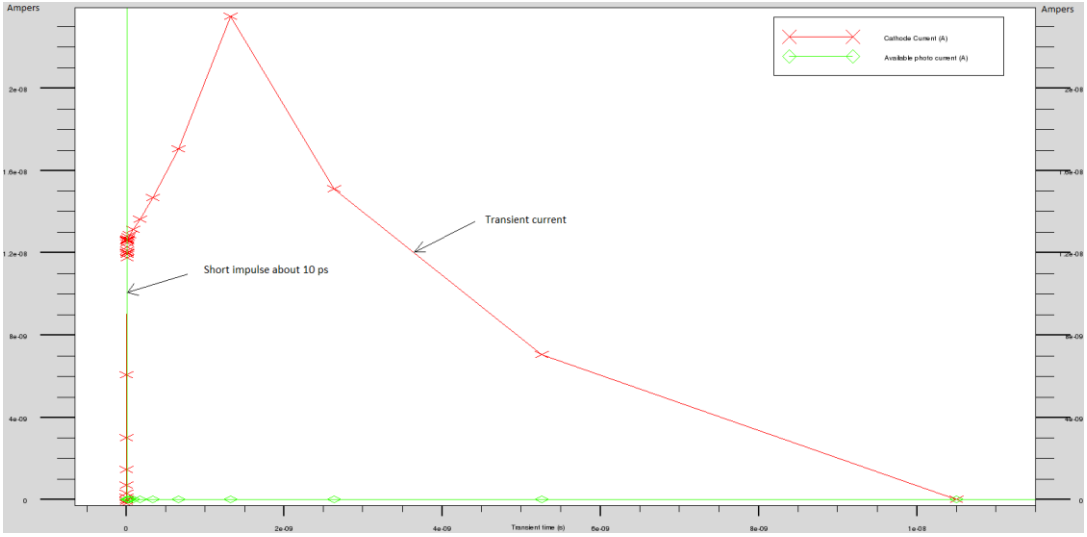

Figure 28. Transient current signal defined 10 ps optical pulse.

6. CONCLUSION

The main topic of this thesis is a study of TCAD simulation framework including MixedMode tool. It was shown, that there are possibilities to use MixedMode circuit simulator not only with electrical sources, but also with other TCAD tools such as Luminous 2D. MixedMode simulation of several circuits ware made. Program way to define those circuits with optical sources and impulses could be found in appendixes 1 and 3.

The aim was to simulate transient current technique setup. The TCT simulation of basic detector and conventional p-type strip detector were carried out. Results of that investigation could be found in corresponding figures. DeckBuild program files created during this work can be used in future researches.

The physics of p-n junction was described with corresponding formulas and semiconductor physics models. Principles of detector work and its internal processes of generation and recombination caused by illumination were dismantled. Principle of construction and work of transient current technique measurement setup was also presented.

REFERENCE

[1] CERN. The Large Hadron Collider. http://home.web.cern.ch/topics/large-hadron-collider. Referred 1.05.2014.

[2] CERN. The Higgs boson. http://home.web.cern.ch/topics/higgs-boson. Referred 1.05.2014.

[3] CERN. The birth of a Higgs boson. http://home.web.cern.ch/about/updates/2013/05/birth-higgs-boson. 1.05.2014.

[4] CERN. How CMS detects particles. http://cms.web.cern.ch/news/how-cms-detects-particles. Referred 2.05.2014.

[5] CERN. CMS Physics. http://cms.web.cern.ch/content/cms-physics. Referred 2.05.2014.

[6] CERN. CMS detector design. http://cms.web.cern.ch/news/cms-detector-design. Referred 2.05.2014.

[7] The CMS tracker: addendum to the Technical Design Report. Technical Design Report CMS. CERN, Geneva, 2000.

[8] V. Eremin, N. Strokan, E. Verbitskaya, and Z. Li. Development of transient current and charge techniques for the measurement of effective net concentration of ionized charges (Nef f) in the space charge region of p-n junction detectors. Nucl. Instrum. Meth., A372:388–398, 1996.

[9] S. M. Sze. Physics of semiconductor devices, 2nd edition. New York, WileyInterscience, 1981.

[10] C. Amsler et al. Review of particle physics. Phys. Lett., B667:1, 2008.

[11] M. Maksimow. Transient current technique characterization of silicon particle detectors. TKK, 2009.

[12] S. Ramo. Currents induced by electron motion. Proc. IRE, 27:584–585, 1939.

[13] G. Kramberger, V. Cindro, I. Mandic, M. Mikuz, and M. Zavrtanik. Determination of effective trapping times for electrons and holes in irradiated silicon. Nucl. Instrum. Meth., A476:645–651, 2002.

[14] J. Harkonen et al. The Cryogenic Transient Current Technique (C-TCT) measurement setup of CERN RD39 Collaboration. Nucl. Instrum. Meth., A581:347– 350, 2007.

[15] V. Eremin, Nucl. Instr. and Meth. A 372 (1996) 388.

[16] V. Eremin, et al., Nucl. Instr. and Meth. A 372 (1996) 188

[17] J. Harkonen et al. RD39 Status Report 2007. Technical Report LHCC-RD-014. CERN-LHCC-2007-028, CERN, Geneva, Nov 2007.

[18] Silvaco, Inc. Atlas User's Manual (device simulation software). November 7, 2013

[19] G. Pellegrini, C. Fleta, F. Campabadal, M. Minano, M. Lozano, J.M. Rafi,M. Ullan, Nucl. Inst. and Meth. A 579 (2007) 599.

[20] G. Casse, P.P. Allport, S. Martiy Garcia, M. Lozano, P.R. Turner, Nucl. Instr. andMeth. A 518 (2004) 340.

[21] S. Marti i Garcia, et al., Nucl. Instr. and Meth. A 426 (1999) 24.

[22] P. Fernandez-Martinez, et al., Simulation of new p-type strip detectors with trench to enhance the charge multiplication effect in the n-type electrodes. Nucl. Instr. and Meth. A 658 (2011) 98–102

[23] G. Lindstrom, et al., Nucl. Instr. and Meth. A 466 (2001) 308.

[24] G. Kramberger, V. Cindro, I. Mandic, M. Mikuz, M. Zavrtanik, Nucl. Instr. And Meth. A 481 (1-3) (2002) 297.

[25] G. Casse, A. Affolder, P.P. Allport, H. Brown, M. Wormald, Nucl. Instr. And Meth. A 624 (2) (2010) 401.

[26] P. Fernández-Martínez, G. Pellegrini, J. P. Balbuena, D. Quirion, S. Hidalgo, D. Flores, M. Lozano, G. Casse . Simulation of new p-type strip detectors with trench to enhance the charge multiplication effect in the n-type electrodes. Nucl. Instr. And Meth. 658(1):98-102. (2011).

APPENDIX 1

DeckBuild program code for MixedMode simulation of basic detector

```
# (c) Silvaco Inc., 2013
#
go atlas
#
# SECTION 1: Mesh Specification
#
mesh space.mult=1.0
x.mesh loc=0.0  spacing=2.5
x.mesh loc=10.0 spacing=2.5
y.mesh loc=0.0   spacing=0.05
y.mesh loc=5.0   spacing=0.2
y.mesh loc=10.0  spacing=0.05
#
# SECTION 2: Structure Specification
#
region num=1 material=Silicon
elec num=1 name=anode x.min=0.0 x.max=10.0 y.max=0.0
elec num=2 name=cathode bottom
doping uniform conc=1e14 n.type
doping gaus peak=0.0 char=0.1 conc=1e18 p.type dir=y
doping gaus peak=10.0 char=0.1 conc=1e18 n.type dir=y
#
trap e.level=0.49 acceptor density=2.e15 degen=12 sign=2.84e-15 sigp=2.84e-14
trap e.level=0.32 donor density=1.e15 degen=1 sign=1.e-16 sigp=1.e-17
#
# SECTION 3: Material Model Specification
#
material taup0=2.e-6 taun0=2.e-6
models srh auger conmob fldmob
#
# SECTION 4: Initial Solution
#
solve    init outf=optoex03_1.str master
tonyplot optoex03_0.str -set optoex03_0.set
#
go atlas
#MixedMode specification (bias)
.begin
r1 1 0 1000
adiod 1=anode 2=cathode infile=optoex03_1.str width=1000
vin 2 0 600
.numeric lte=0.05
.options fulln print
.save outfile=optotest50
.log outfile=optotest50
.end
#MixedMode specification ends (bias)
models device=adiod conmob fldmob surfmob srh auger bgn print
method newton autonr trap
```

```
go atlas
#MixedMode specification (optical impulse)
.begin
r1 1 0 1000
opt1 1 0 pulse 0 10 10ns 0.001ns 0.001ns 100ns 10
adiod 1=anode 2=cathode infile=optoex03_1.str width=1000
vin 2 0 5
# MixedMode specification ends (optical impulse)
.numeric dtmin=0.1ps lte=0.5
.load infile=optotest50
.save outfile=optotest50_tr
#
.options fulln print
#
.log outfile=optotest50
#
.tran 1ns 200ns
#
.end
#
beam num=1 x.origin=5.0 y.origin=11.0 angle=-90.0 wavelength=.623
models device=adiod conmob fldmob surfmob srh auger bgn print
method newton autonr trap

go atlas
tonyplot optotest50_tr.log
quit
```

APPENDIX 2

DeckBuild program code for structure simulation of conventional p-type stripped detector

```
go athena
# The X mesh definition
line x loc=0.00 spac=1
line x loc=160 spac=1
# The Y mesh definition
line y loc=0.00 spac=0.1
line y loc=1 spac=0.1
line y loc=1.5 spac=0.01
line y loc=2 spac=0.1
line y loc=5 spac=1
line y loc=20 spac=5
line y loc=50 spac=10
line y loc=100 spac=20
line y loc=250 spac=20
line y loc=285 spac=1
# The doping of silicon substrate is given by
init silicon c.boron=1.0e12 orientation=100 two.d
# Nitride deposition for uniform boron implantation
deposit nitride thick=0.05 divisions=2
# Boron implantation for addition hole concentration on the top
implant boron dose=3e10 energy=120 tilt=0 rotation=0 crystal
# Annealing process for uniform distribution of the implanted boron
di
us time=120 temp=1200 nitro press=1.00
# The all nitride etch process
etch nitride all
# Nitride deposition for uniform boron implantation
deposit nitride thick=0.05 divisions=2
# Oxide deposition for p stop boron implantation
deposit oxide thick=2 divisions=2
# The oxide etch process for p stop boron implantation
etch oxide start x=36 y=-2.05
etch cont x=44 y=-2.05
etch cont x=44 y=0
etch done x=36 y=0
# The oxide etch process for p stop boron implantation
etch oxide start x=116 y=-2.05
etch cont x=124 y=-2.05
etch cont x=124 y=0
etch done x=116 y=0
# Boron implantation for p stop region
implant boron dose=1.0e16 energy=80 tilt=0 rotation=0 crystal
ii
# Annealing process for uniform distribution of the implanted boron
di
us time=60 temp=1100 nitro
# The all oxide etch process
```

```
etch oxide all
# The all nitride etch process
etch nitride all
# Nitride deposition for uniform phosphor implantation
deposit nitride thick=0.05 divisions=2
# Oxide deposition for n+ phosphorus implantation
deposit oxide thick=2 divisions=2
# The oxide etch process for n+ phosphorus implantation
etch oxide start x=64 y=-2.05
etch cont x=96 y=-2.05
etch cont x=96 y=0
etch done x=64 y=0
# The oxide etch process for n+ phosphorus implantation
etch oxide left p1.x=16
# The oxide etch process for n+ phosphorus implantation
etch oxide right p1.x=144
# Phosphor implantation for n+ region
implant phosphor dose=1e15 energy=100 tilt=0 rotation=0 crystal
# Annealing process for uniform distribution of the implanted phosphorus
di
us time=60 temp=1060 nitro
# The all oxide etch process
etch oxide all
# The all nitride etch process
etch nitride all
# Inverting structure for the bottom side processing
structure flip.y
# Boron implantation for p+ region on the bottom side
implant boron dose=1.0e17 energy=80 tilt=0 rotation=0 crystal
# Annealing process for uniform distribution of the implanted boron
di
us time=60 temp=1050 nitro
# Inverting structure for the top side processing
structure flip.y
# Oxide deposition for electric contact processing
deposit oxide thick=2 divisions=2
# The oxide etch process for electric contact processing
etch oxide start x=72 y=-2
etch cont x=88 y=-2
etch cont x=88 y=0
etch done x=72 y=0
iii
# The oxide etch process for electric contact processing
etch oxide left p1.x=8
# The oxide etch process for electric contact processing
etch oxide right p1.x=152
# Aluminum deposition for creating the electrodes
deposit aluminum thick=2 divisions=2
# The aluminum etch process for creating the electrodes
etch aluminum start x=10 y=-4
etch cont x=70 y=-4
etch cont x=70 y=-2
etch done x=10 y=-2
# The aluminum etch process for creating the electrodes
```

```
etch aluminum start x=90 y=-4
etch cont x=150 y=-4
etch cont x=150 y=-2
etch done x=90 y=-2
# Defining of the cathode
electrode name=cathode x=1 y=-1
# Defining of the cathode
electrode name=cathode x=80 y=-1
# Defining of the cathode
electrode name=cathode x=159 y=-1
# Defining of the anode
electrode name=anode backside
# Saving the created structure
struct outfile=conv det.str
# Plotting the structure
tonyplot conv det.str
# Exit from the code
quit
```

APPENDIX 3

DeckBuild program code for MixedMode simulation of conventional p-type stripped detector

```
go atlas
.begin
r1 1 0 1000
adiod 1=anode 2=cathode infile=conv_ptype_det_normal.str width=1000
vin 2 0 10
.numeric lte=0.5
.options fulln print
.save outfile=optotest7
.log outfile=optotest7
.end
models device=adiod conmob fldmob surfmob srh auger bgn print
method newton autonr trap
go atlas
.begin
r1 1 0 1000
opt1 1 0 pulse 0 10 10ns 0.001ns 0.001ns 100ns 10
adiod 1=anode 2=cathode infile=conv_ptype_det_normal.str width=1000
vin 2 0 10
#
.numeric dtmin=0.1ps lte=0.5
.load infile=optotest7
.save outfile=optotest7_tr
#
.options fulln print
#
.log outfile=optotest7
#
.tran 1ns 200ns
#
.end
#
beam num=1 x.origin=80.0 y.origin=301 angle=-90.0 wavelength=.623
models device=adiod conmob fldmob surfmob srh auger bgn print
method newton autonr trap

go atlas
tonyplot optotest7_tr.log
quit
```